Master's thesis

NTNU
Norwegian University of Science and Technology
Faculty of Information Technology and Electrical Engineering
Department of Electric Power Engineering

Magnus Normann Johannessen

Influence of voltage frequency and rate of change on internal partial discharges

Master's thesis in Energy and Environmental Engineering
Supervisor: Pål Keim Olsen
Co-supervisor: Espen Eberg
June 2022

NTNU
Norwegian University of
Science and Technology

Magnus Normann Johannessen

Influence of voltage frequency and rate of change on internal partial discharges

Master's thesis in Energy and Environmental Engineering
Supervisor: Pål Keim Olsen
Co-supervisor: Espen Eberg
June 2022

Norwegian University of Science and Technology
Faculty of Information Technology and Electrical Engineering
Department of Electric Power Engineering

NTNU
Norwegian University of
Science and Technology

Abstract

Internal partial discharges in electric machine insulation represents a significant source of degradation, ultimately leading to breakdown. High voltage machines are, to an increasingly degree, exposed to fast repetitive voltage pulses caused by transistor-switching in power electronic converters. An understanding of how such high-voltage pulses affects the behaviour of partial discharges is therefore necessary.

The purpose of this thesis is to investigate and explain how the behaviour of partial discharges are affected by high-voltage pulses with short rise times, compared with sinusoidal voltage. To answer this, a partial discharge prediction model is developed that expands on the well-known capacitance model, in addition to experimental measurements performed on test objects with various void gap distances. Experiments are performed on mica-epoxy groundwall insulation with cylindrical cavities at voltages slightly above the inception voltage levels, and a high-frequency transformer connected to an oscilloscope is used to measure the discharges. The partial discharge characteristics of interest are the repetition rate and magnitude, as well as the phase-distribution of the discharges.

The capacitance model is expanded to include a frequency-dependent statistical time lag and remanent voltage, and a residual charge decay. Compared to the experimental results, qualitatively similar results are achieved in some of the investigated characteristics, although other aspects differ greatly. A significant numerical difference is observed, which is mainly thought to stem from the simplifications made in regards to discharge types and changing void surface characteristics.

Sammendrag

Interne, partielle utladninger i elektriske maskiner utgjør en betydelig kilde til degradering og havari. Høyspentmaskiner blir i økende grad utsatt for raske, repetitive spenningspulser forårsaket av transistor-switching i kraftelektronikk. En grundigere forståelse av hvordan slike høyspentpulser påvirker adferden til partielle utladninger er derfor nødvendig.

Målet med denne avhandlingen er å undersøke og forklare hvordan adferden til partielle utladninger blir påvirket av høyspentpulser med korte stigetider, sammenlignet med sinusspenning. For å svare på denne problemstillingen har en utladningsmodell, bygget på den kjente kapasitive modellen, blitt utviklet. I tillegg er det gjennomført eksperimentelle forsøk på prøveobjekter med ulike hulromstykkelser laget av mica-epoxy generatorisolasjon med sylindriske hulrom. Forsøkene er gjennomført med spenningsamplituder like over tennspenningene, og utladningene er målt med en høyfrekvent strømtransformator koblet til et oscilloskop. Utladningsegenskapene som er av interesse er repetisjonsraten og størrelsen, i tillegg til faseposisjonen til utladningene.

Den kapasitive modellen er utvidet til å inkludere en frekvensavhengig statistisk tidsforsinkelse og remanent spenning, og en avtagende restladning. Sammenlignet med de eksperimentelle måleresultatene klarer modellen å beskrive enkelte deler av adferden til utladningene, mens andre deler er svært ulike. De numeriske verdiene er svært ulike, noe som antas å skyldes de forenklingene som er gjort knyttet til utladningstype og endringer i overflateegenskaper i hulrommet.

Preface

This master thesis is submitted in partial fulfillment of the requirements for the degree of Master of Science in Engineering (MSc) at the Norwegian University of Science and Technology (NTNU) in Trondheim, Norway. The work has been carried out at the Department of Electric Power Engineering between January and June 2022. Associate Professor Pål Keim Olsen has been the main supervisor for this work, with Espen Eberg (SINTEF) as co-supervisor.

The work was part of the SINTEF KPN project (knowledge-building project for industry) "FastTrans", funded by the Research Council of Norway. The project partners are NTNU, University of Bologna, Infineon, Statnett SF, Equinor Energy AS, ABB AS, Statkraft Energi AS, Elvia, Aker BP AS, and Total E&P NORGE AS.

Trondheim, June 2022

Magnus Normann Johannessen

Acknowledgements

I want to express my gratitude to my supervisor, Pål Keim Olsen, and co-supervisor Espen Eberg, for their constructive feedback and guidance along the way, as well as pointing me in the right direction when stuck. I would also like to thank Torstein Grav Aakre for the help that he has provided me on the laboratory, as well as feedback on my work. His experience and knowledge has been of great value. Lastly, I would like to thank my fellow students at room F-322 for the many laughs and good conversations we have shared this past year.

Contents

Chapter 1

Introduction

1.1 Background

Wind energy power conversion is set to play a central part in the clean electrification of transport and industry towards 2050, following a rapid rise in recent years. In the last decade, the full variable speed synchronous generator with a 100% capacity power converter has gained popularity in the wind energy market, simultaneously with a shift towards higher power ratings. The increased power ratings have also pushed the voltage from low voltage (690 V) up to medium voltage (<3 kV)[1, 2].

The combination of fast voltage pulse switching in the power converters and medium voltage amplitude presents a challenge for the insulation materials within the generator. The effects may be a decrease in generator lifetime, a decrease in generator power-to-weight ratio or conservative insulation system designs [3–5].

This master thesis is done as part of the *FastTrans* project, an ongoing research project at SINTEF Energy Research and NTNU. The FastTrans project looks at stresses on various types of insulation materials caused by fast voltage transients from high voltage power electronics. Such converters are central elements in the physical infrastructure of any flexible energy system because they enable efficient switching and seamless control of the power flow between the suppliers and consumers in the electric power grid. However, the transient voltage rise times cause more stress on the electric insulation than conventional 50 Hz sinusoidal voltage, on which the industry's factory acceptance stress tests are largely based [1, 6].

The FastTrans project focuses on three specific R&D challenges that are important for the development of generic test standards [7]:

- Partial discharge occurrence and detection
- Pulse propagation in networks into components
- Ageing diagnostics

This thesis focuses on the first part, namely partial discharge (PD) occurrence and detection. More specifically, it will look at the occurrence of PDs in electric machine insulation when repetitive high voltage pulses with short rise times (<300 ms) and high voltage-frequencies (<4 kHz) are applied.

1.2 Literature review

The following literature survey was performed as part of the specialisation project [1] and is included to give the reader a better understanding of the background of the thesis.

A 2005 review article from Morshuis concluded that "PD induced degradation and how they are affected by voltage of higher frequency, distorted voltages and repetitive transients ask for more attention" [8]. Many investigations since then have qualitatively studied the effects of increased voltage frequency and voltage waveform on the lifetime of the stator winding insulation [3, 9–14], but fail to explain quantitatively the frequency-dependence of the PDs that leads to insulation degradation. Early papers by Ul Haq *et al.* [3] compared 60 Hz ageing with 3 kHz pulse ageing on mica-based groundwall insulation and concluded that pulse ageing was more severe. Meanwhile, Chen *et al.* [10] found that mica groundwall insulation did not experience any shorter lifetime at 14 kHz PWM voltage than at 60 Hz AC voltage. Even though a decrease in lifetime with increased voltage frequency is shown, Manns *et al.* [9] argues that the number of voltage cycles is the predominant ageing factor. Moonesan *et al.* [14] later showed that the time-to-failure decreased linearly with the number of cycles up to 750 Hz and less linearly above this for both unipolar and bipolar waves. They also showed that the time-to-failure under bipolar square waves was longer than for unipolar waves.

An understanding of the mechanisms behind PDs is necessary to understand the phenomena and its dependence on voltage parameters such as frequency, amplitude and rise time. Early work by Niemeyer [15] presented a generalised model to explain the relation between insulation defect characteristics and measurable PD characteristics. A paper the following year by Morshuis and Niemeyer [16] presented the discharge mechanisms behind PDs in flat delamination voids. Gäfvert *et al.* [17] later investigated the influence of statistical time lag on the frequency-dependence of the PD pattern using a capacitance model and found that this could be used to interpret PD patterns under variable voltage frequency. However, the capacitance model has been criticised for not representing the physical process that occurs within a real system [18].

With increased computational power and the improvement of Field Element Analysis (FEA) software, alternative models have also received attention. Forssén and Edin [19, 20] studied PDs in cylindrical voids in polycarbonate at variable frequency between 0.1 - 100 Hz and used Comsol Multiphysics® to simulate their model. They found that the PD frequency-dependence changed with the applied

voltage amplitude, cavity diameter and cavity location. They suggested that the PD frequency-dependence was governed by the statistical time lag and surface charge decay. They also found that surface conductivity and surface emission of electrons change with varying frequencies. Illias *et al.* [21] presented a stochastic simulation model for spherical voids in epoxy resin, implemented in FEA software, and found a correlation between applied voltage frequency, voltage amplitude and PD repetition rate in the frequency range 1-50 Hz. Borghei and Ghassemi [18] presented a Finite Element Model of PD activity in spherical voids under square wave voltage with even higher frequencies of 3 kHz. They concluded that as the voltage frequency increases, the voltage-level at which PDs occur decreases and the discharge repetition rate increases.

Callender [22] presented a model of plasma dynamics of PD activity in a cylindrical void. He found that the model was in acceptable agreement with experimental data. However, only voltage amplitudes up to 2.2 kV and frequency of 50 Hz were considered.

These works show that while a lot has been done to understand the mechanisms governing PDs in internal voids, experimental data is still limited on the impact of high-frequency transients. One crucial challenge is the variety in investigated voids and dielectric materials, making generalisation and comparisons challenging. Even so, unipolar and bipolar square wave voltages with high frequency have been shown to impact the lifetime of groundwall insulation, highlighting that there is still a need for further investigations.

1.3 Research objective

Although extensive research has been done into the effects of high-voltage, low-frequency sine wave voltage on PD behaviour, little is still understood about the effects of repetitive high-voltage transients. Many studies have, as mentioned, observed more severe ageing at higher frequencies. Therefore, more research into the effects of voltage frequency and rise time on PD behaviour is warranted. This thesis aims to experimentally and theoretically investigate the relations between measurable voltage- and PD parameters. The voltage parameters of particular interest are the frequency and the rate of change.

Tests are performed using multiple laboratory test objects with known cylindrical void geometries. The model is developed based on the capacitive abc model, but expanded to include the effects of time lag, charge decay and various remanent voltage. In order to provide a meaningful research contribution to the fields of partial discharge modelling and measurement, the thesis critically evaluates both the experimental techniques and the modelling approach.

The main objective of the thesis can be summarised as follows:

Explain the voltage frequency and rate of change -dependence of experimental PD results in cylindrical generator insulation voids.

1.4 Methodological approach

PDs, especially in closed internal voids, are fundamentally challenging to examine. Firstly, it is impossible to measure the discharges directly due to the enclosed void. Secondly, there are numerous parameters affecting the behaviour of the PDs. Any model describing PD behaviour must therefore include certain simplifications and be transparent in its limitations.

Due to the difficulty in estimating specific input parameters, the work done in this thesis can be described as an inductive research approach where experimental measurements are performed to obtain empirical data from which patterns can be analysed in order to obtain theoretical knowledge. Existing theory and empirical data forms a foundation on which an expanded capacitive model is developed. Measurements are performed on multiple test objects to obtain data on how the PD behaviour changes with voltage frequency and voltage rate of change. Model input-parameter values are selected to achieve a similar pattern as the measurement results, and the results are then compared and discussed in order to answer the research objective.

1.5 Outline of the thesis

Chapter 1 presents the background for the thesis project along with the research objective and overall methodological approach used to address the objective. Chapter 2 presents existing theoretical knowledge about PDs in internal voids and the physical parameters that are later used to create a PD prediction model. Chapter 3 outlines the design of the model along with suggested equations for describing a frequency-dependence in the physical parameters presented in Chapter 2. The experimental methods are described in Chapter 4; this includes the test objects, laboratory setup, test procedure and post-treatment of the measured data. The measured and simulated results are presented, compared and discussed in Chapter 5. Some important observations are discussed as they are presented, while a broader discussion and evaluation is done at the end of the chapter. Here, sources of error in both the modelling and measurements are discussed along with suggested improvements. Chapter 6 presents the conclusion to the thesis objective, and lastly Chapter 7 contains suggestions to further work.

Chapter 2

Theory

This chapter expands on the theoretical foundation in the specialisation project [1] and presents the necessary background knowledge to explain the model and the experimental results.

2.1 Modelling of a void

At low voltage frequencies, the PD inception voltage (PDIV), which is the lowest voltage fulfilling the required conditions for sustained PDs to occur, is highly dependent on the conductivity and permittivity of the material. However, at higher voltage frequencies, the effect of void conductivity on PDIV is negligible as it is highly permittivity-dominated. Frequency-dependent resistance can, at frequencies well above 100 Hz, be disregarded [23]. Doing so allows for a simple equivalent circuit where the three central elements are modelled through capacitances; the void (c), the dielectric between the electrode and the void (b), and lastly, the remaining dielectric surrounding the void (a). This model is referred to as the *abc model* or *capacitance model* [24]. When the required conditions are met, a short-circuit occurs in the void leading to a sudden drop in voltage. Figure 2.1.1 illustrates this model.

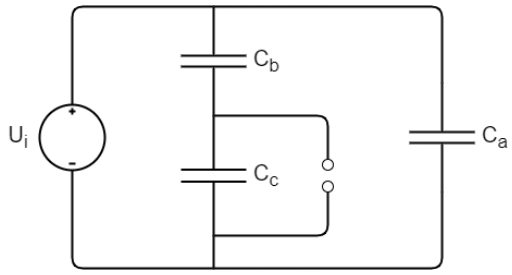

Figure 2.1.1: Equivalent circuit model

The relation between the void voltage U_v and applied voltage U_i can be found using the voltage division in Equation 2.1,

$$U_i = \left(1 + \frac{d_b}{d_c} \cdot \frac{\epsilon_c}{\epsilon_b}\right) \cdot U_v \tag{2.1}$$

where d_c is the height of the void (void gap distance), d_b is the section of dielectric material in series with the void, ϵ_c is the void gas permittivity, and ϵ_b is the dielectric permittivity.

The capacitive abc model is built on four central assumptions [23]:

- The electric field inside the void is homogeneous.
- A PD event occurs when the void voltage reaches the breakdown voltage level. There is no time delay between reaching the critical breakdown level and the start of a PD.
- The entire electrode area of the void is discharged.
- The residual charge left on the void surface after a PD event remains constant between discharges. There is no charge decay between the discharges.

These are helpful simplifications, although not necessarily a true reflection of the behaviour in such voids. These assumptions will be addressed in the following sections, and chapter 3 will address the efforts made to increase the complexity of the model.

2.2 Partial discharges under alternating voltage

PDs occur due to the local electric field exceeding the breakdown field strength of the given material. In electrical machines, internal gas bubbles in the insulation materials, which occur due to various imperfections, represent a significant source for PDs [24]. Due to the low permittivity of the gas relative to the dielectric, the gas will experience a much greater electric stress than the dielectric. In high-voltage (HV) machines, this leads to a continuous PD activity in the insulation, which ultimately represents a significant source of ageing and degradation.

For a PD to occur, two conditions need to be fulfilled: the local electric field strength must exceed the breakdown field strength, and there needs to be a free electron available to start the ionisation process [15]. Both these criteria are highly dependent on factors such as void geometry, void surface characteristics, and the applied voltage, and they will be explained in turn on the following sections.

The occurrence of PDs is illustrated through a sudden drop in the voltage across the void, as shown in Figure 2.2.1. Here, U_v^0 is the void voltage if no PDs occur, and U_v is the actual void voltage if PDs do occur. When the void voltage exceeds the critical limit $U_{paschen}$, which will be explained further in section 2.3, a drop in void voltage will occur; the voltage drop corresponds to a charge of electrons across the void. By applying a different voltage shape with a shorter rise time, the PDs will occur earlier in the phase, as shown in Figure 2.2.2. As the voltage rate of change is significantly higher, the void voltage will rise to the critical Paschen voltage much faster than with sine wave voltage, leading to a much shorter time between consecutive discharges.

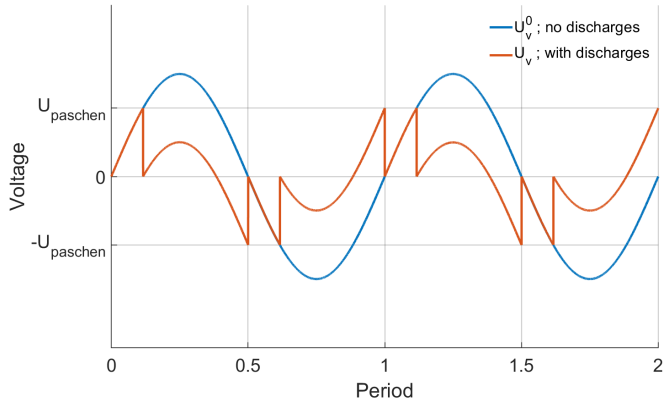

Figure 2.2.1: Drop in void voltage U_v when a sine wave voltage is applied

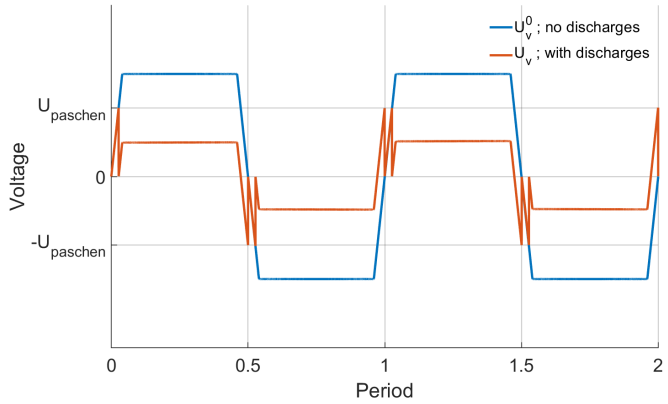

Figure 2.2.2: Drop in void voltage U_v when a square wave voltage is applied

2.3 Electric field strength and voltage

The requirement of critical field strength is well documented and described through the Paschen voltage for air. The electric field inside the void needs sufficient strength for a PD to initiate. The critical field strength is dependent on the pressure and volume of the void gas and is described through the equation

$$E_{crit} = \left(\frac{E}{p}\right)_c \cdot p \cdot \left(1 + \frac{B}{\sqrt{p \cdot d_c}}\right) \tag{2.2}$$

where $(E/p)_c$ is the pressure reduced critical field, p is the pressure within the void, and B is a constant [25]. The gas within the void is often assumed to be air with atmospheric pressure, although in reality the gas will ionise as a consequence of the PDs, leading to the creation of ozone gas and a slight change in pressure. By assuming no change in gas characteristics, Equation 2.3 can be used to find the critical voltage level,

$$U_{paschen} = 2.436(\rho_0 \cdot d_c) + 2.125\sqrt{\rho_0 \cdot d_c} \tag{2.3}$$

where d_c is given in mm and $U_{paschen}$ is given in $\mathrm{kV_{peak}}$. The two values 2.436 and 2.125 are derived from $(E/p)_c$ and $\sqrt{K/C}$ respectively. The applied values are E=24.36 kV/cm, p=1 bar and K/C=45.16 $\mathrm{kV^2/(cm{\cdot}bar)}$ [26]. ρ_0 is the ratio between pressure and temperature of the air relative to 1 bar and 0 degrees Celsius:

$$\rho_0 = \frac{p}{1.1013 \times 10^5} \cdot \frac{293}{T} \tag{2.4}$$

2.4 Time lag

The requirement of an available free electron to initiate the electron avalanche causes variability in discharge magnitudes due to the innate randomness of the availability. This randomness leads to a variable time delay from the moment of critical field strength until the discharge event, allowing the field strength to increase to a level above the critical level, thus affecting the voltage drop magnitude. Free electrons may be generated by volume generation or surface generation within the void [15]. In the case of cylindrical internal voids, surface generation through detrapping of electrons from the void surface is the dominant source of free electron generation [25]. This source closely obeys the Richardson-Schottky scaling [15, 25]:

$$\dot{N}_{es}(t) = \frac{S_{void}}{e} \cdot S_{det} \cdot exp\left(-\frac{\Phi - \sqrt{e^3 E/(4\pi\epsilon_0)}}{k_b T}\right)\left(1 - \frac{\eta}{\alpha}\right) \tag{2.5}$$

where S_{void} is the void surface area, e is the elementary charge, S_{det} is the function in surface emission law, Φ is the effective work function, k_b is the Boltzmann constant, and (1-$\frac{\eta}{\alpha}$) is the Legler function. The surface emission law is given as

$$S_{det} = v_0 \cdot e\frac{N_{dt}}{S_{void}} \tag{2.6}$$

where v_0 is the fundamental photon frequency and N_{dt}/S_{void} is the surface density of detrappable charges. The implementation of this effect is usually done with a time lag, which is the inverse of the electron generation rate. For simplicity, this time lag is modelled through an exponential probability distribution [17, 23, 25, 27]. The probability density function (PDF) is illustrated in Figure 2.4.1, and the cumulative distribution function is given in Equation 2.7.

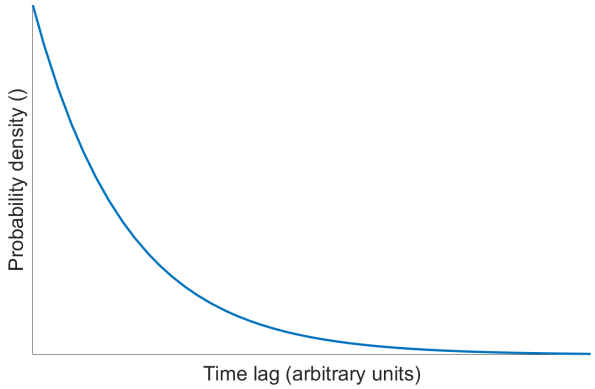

Figure 2.4.1: Time lag probability density

$$P_d = \begin{cases} 1 - exp\left(-\frac{\tau_s}{t_L}\right) & E_{void} \geq E_{crit} \\ 0 & E_{void} < E_{crit} \end{cases} \tag{2.7}$$

τ_s is the statistical time lag corresponding to the mean waiting time, and t_L is the time passed since the void field strength exceeded the critical field strength. The time lag values are calculated by solving the cumulative distribution function (CDF) to find t_L, which is then compared with a random number between 0 and 1 [27]:

$$t_L = -\tau_s \cdot ln(1 - R) \tag{2.8}$$

The void voltage at the time of discharge with a sine wave voltage can then be found using Equation 2.9.

$$U_v = U_v^0 \cdot sin(2\pi f(t_p + t_L)) \tag{2.9}$$

where t_p is the moment when the void voltage reaches the critical level. The time lag can be implemented in a square wave voltage in the same way using Equation 2.10, where f_{sq} is the square wave function.

$$U_v = U_v^0 \cdot f_{sq}(t_p + t_L) \tag{2.10}$$

The effect of time lag is visualised in Figure 2.4.2 with a square wave voltage, where some discharges occur close to the critical Paschen voltage while others occur at a much higher voltage level. Unlike a sine wave voltage which changes continuously, (an ideal) square wave voltage will maintain its maximum amplitude for a longer time. This means that a higher number of discharges will have a very similar magnitude as long as they do not occur in the rise or fall flank.

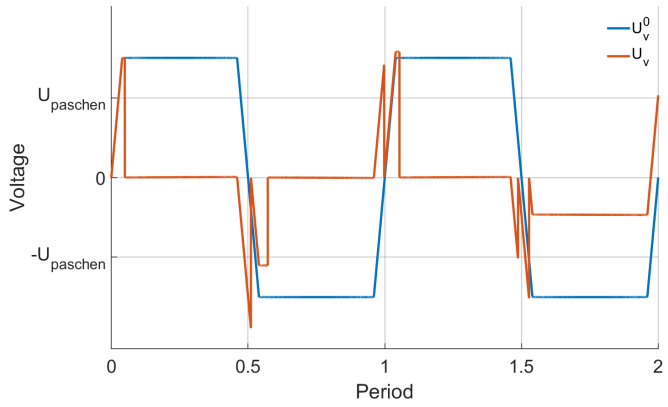

Figure 2.4.2: Effects of stochastic time lag on void voltage

The selection of statistical time lag greatly influences the phase-position of the discharges and, thereby, the discharge repetition rate. For example, a short statistical time lag relative to the voltage period causes PDs to occur close to the critical Paschen voltage-level. Similarly will a long statistical time lag relative to the voltage period cause PDs to be shifted forward in phase and occur at higher voltage levels than the critical voltage. This statistical effect results in fewer PDs per voltage period and larger magnitudes when the statistical time lag increases relative to the voltage period. Consequently, this causes a frequency dependence in PD behaviour as the period time decreases with increasing frequency [19].

2.5 Charge decay

Surface conduction and recombination, as well as diffusion of electrons into surface traps, leads to a charge decay within the void after a discharge event. This charge decay reduces the field enhancement close to the zero-crossings of the applied voltage, thereby shifting the PDs forward in phase and reducing the number of PDs per voltage cycle [19]. The rate at which the charges decay depends on the geometry and conductivity of the void surface. The impact of charge decay largely depends on the relative difference between the charge decay rate and the voltage rate of change. If the decay is very slow relative to the voltage rate of change, the effects will be less than if otherwise. The decay would also affect the time lag due to the gradual reduction of free electrons after a PD event. A high residual charge would leave free electrons from a PD event available to initiate a new PD event, reducing the waiting time. The residual charge is represented by a *residual voltage* continuously decreasing due to the decay, and this effect can be illustrated in Figure 2.5.1.

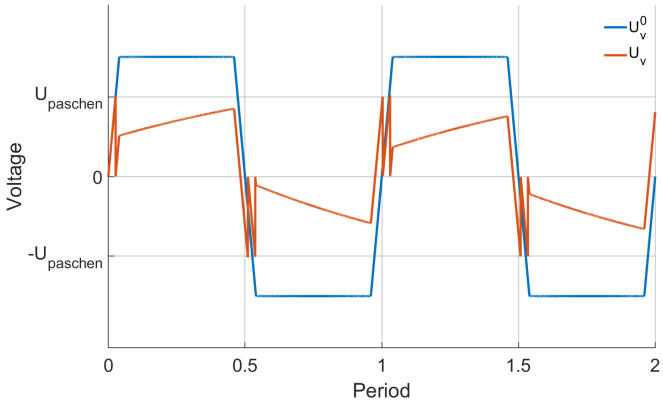

Figure 2.5.1: Effects of charge decay on void voltage

2.6 Remanent voltage

The voltage level that U_v drops to after a PD event is referred to as the *remanent voltage* and corresponds to the charge level left over immediately after a PD event. This should not be confused with the residual voltage, which represents the actual charge level in the void at any given time.

PDs are typically categorised as either Townsend-type or streamer-type. A Townsend-type discharge is characterised by a self-sustaining discharge started by a first electron and sustained by a feedback mechanism, where positive ions travel back to the cathode where they produce secondary starting electrons. A relatively large section of the void surface area is discharged, and the PD event stops when the residual field reaches a specific value, which is often close to the critical field strength [16]. The streamer-type discharge is a self-channelling ionisation process driven by a space charge distorted electric field [15]. Successive avalanches are created by high-speed photons, making the streamer-type discharges propagate faster than the Townsend-type discharges. It is also more localised but may ignite several parallel streamer channels due to the photoionisation feedback. The high field strength on the ends of the positive streamers also makes the streamer-like discharge more avalanche-sustaining, leading to a lower residual charge close to zero [27]. The discharge type is thought to be governed by the overvoltage above the critical level for a discharge to occur [28]. The following highlights the core differences [27]:

Townsend-type	**Streamer-type**
• Low overvoltage	• High overvoltage
• Remanent voltage close to breakdown voltage	• Remanent voltage close to zero
• Cover a large part of the cavity surface	• Cover a small part of the cavity surface
• Low discharge magnitude	• High discharge magnitude

Both these discharge types will be present in internal voids, leading to a spread of discharges with varying magnitude and duration. The discharge type is, determined by factors such as the magnitude of the overvoltage above the Paschen voltage, geometry of the void and the field distribution inside the void. Internal voids exposed to alternating voltage will therefore contain a distribution of PD magnitudes, not only due to the statistical effects mentioned, but also due to the variability of the discharge type.

2.7 Apparent charge

PDs can not be measured directly, and it is therefore necessary with indirect methods of measurement. This is done by measuring the effects of the PDs on the voltage in the external circuit; when a PD occurs, a transient voltage drop also occurs across the test object [24]. This voltage drop is typically measured using a capacitor in parallel with the test object and measuring the PDs' effect on the voltage. The charge corresponding to this voltage drop is the apparent charge q_a. The discharge magnitude in the capacitance model is given in Equation 2.11 as the product of the series dielectric capacitance C_b and the magnitude of the voltage drop, ΔU_v.

$$q_a = \left(C_a + \frac{C_b \cdot C_c}{C_b + C_c}\right) \cdot \left(\frac{C_b}{C_b + C_c}\right) \cdot (U_{ign} - U_{rem}) \approx C_b \cdot \Delta U_v \tag{2.11}$$

The simplification performed here is valid if $C_b << C_c$ or (C_b and C_c) $<< C_a$ [23]. The series dielectric capacitance for cylindrical voids is found as

$$C_b = \epsilon_0 \cdot \epsilon_b \cdot \frac{A_b}{d_b} \tag{2.12}$$

where ϵ_0 is the vacuum permittivity, and A_b is the dielectric area facing the void, equal to the void's surface area.

Chapter 3

Stochastic model design

The work done in this thesis consists of two parts: the experimental work and the theoretical model. This chapter explains the modelling work in detail. First, the model flowchart is presented, followed by an explanation of the various input parameters. Then, equations for a frequency-dependent statistical time lag and remanent voltage are suggested to describe the change in PD behaviour at increasing frequency. For the complete model code implemented in Matlab, see Appendix C.

3.1 List of assumptions

The following assumptions are made due to the necessity to simplify the modelling process. The impact of these will be discussed further in chapter 5.

- The electric field inside the void is homogeneous.
- A statistical time lag, τ_s, leads to a time delay between reaching the critical breakdown level and the start of a PD. τ_s changes with voltage frequency and rate of change.
- The residual charge left over after a PD event decays with a constant, exponential rate.
- The entire void-area discharges during a PD event, meaning that only Townsend-type discharges are considered. During a PD event, the void voltage drops to a remanent voltage level U_{rem}; the remanent voltage level is determined by the voltage frequency and rate of change.

3.2 Flowchart

Figure 3.2.1 and Figure 3.2.2 shows a flowchart of the model for use with sine wave and square wave voltage respectively. Apart from the voltage function and the input parameters necessary to create the voltage function, the steps are the same. The input parameters are defined with constants. First, an initial time lag value is created, and the first iteration is set with $t = 0$ and U_{res}=0. The time step is updated at the beginning of each iteration. The void voltage in the current time-step is found first. If the voltage in the current time-step is higher than the Paschen voltage, and the time passed since the Paschen-voltage crossing is longer than the time lag, a discharge is allowed to occur. The time-step of the discharge is stored in a vector t_q, and the magnitude of the voltage drop is calculated. Then the residual voltage is updated, and the discharge magnitude is calculated. A new time lag is calculated before the time since previous discharge is found. Lastly, a charge decay value is implemented on the residual voltage.

If the discharge criteria are not met in the current time-step, a check for polarity change is performed. If the polarity of the current time-step is equal to that of the previous time-step, the time since previous discharge is found. If there is a polarity change between the time-steps, a new time lag is calculated before the time since previous discharge is found.

Finally, when the time-step reaches the end of the time vector, the code exits the feedback loop and vectors for discharge magnitude and timestamps are assembled.

The entire model is run 18 times in parallel to account for the statistical effects of time lag. As the time lag values are not normally distributed, it was not possible to present the results in the form of confidence intervals. Therefore, the average value of all 18 simulations is used in the analysis.

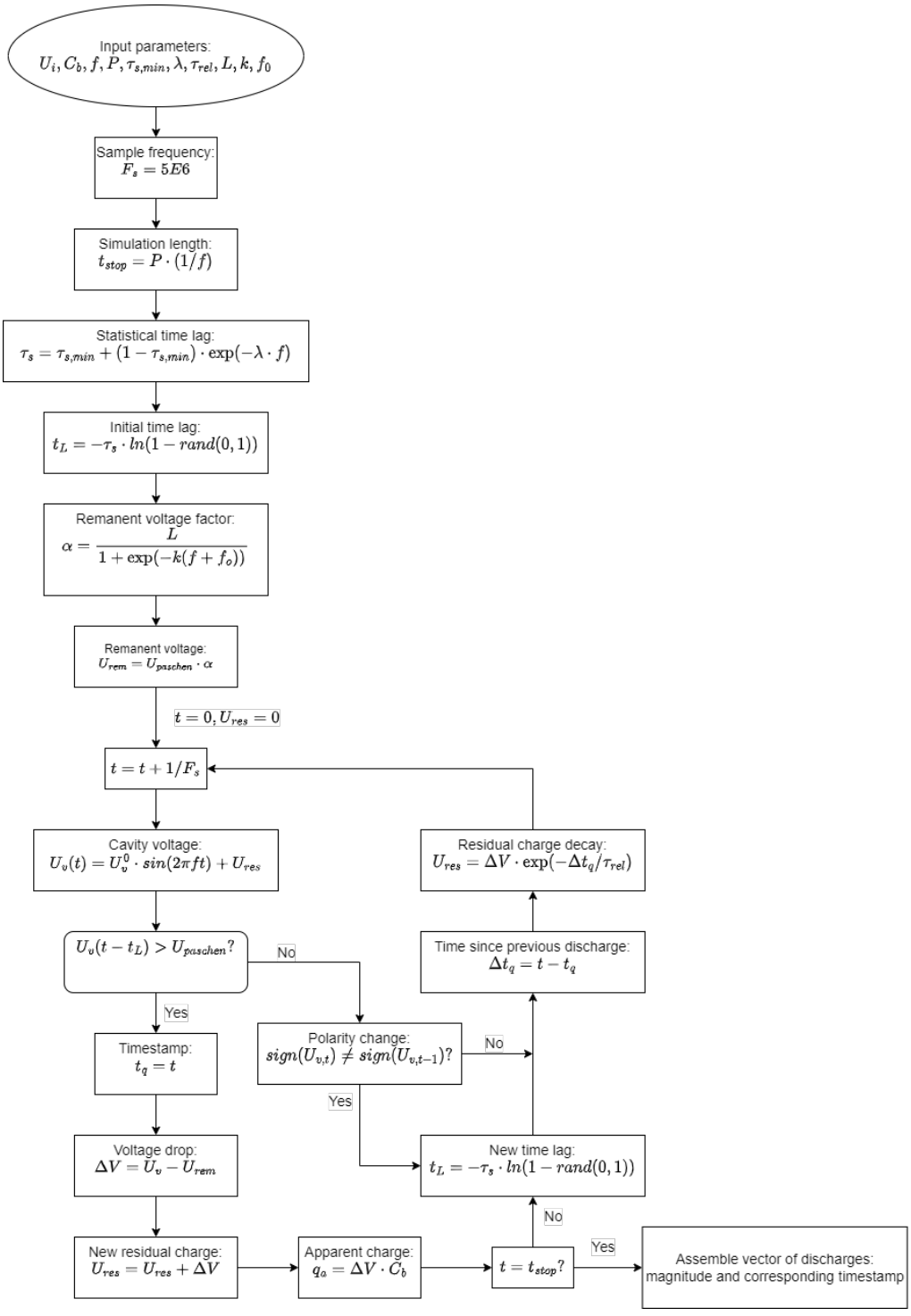

Figure 3.2.1: Flowchart of model with sine wave voltage

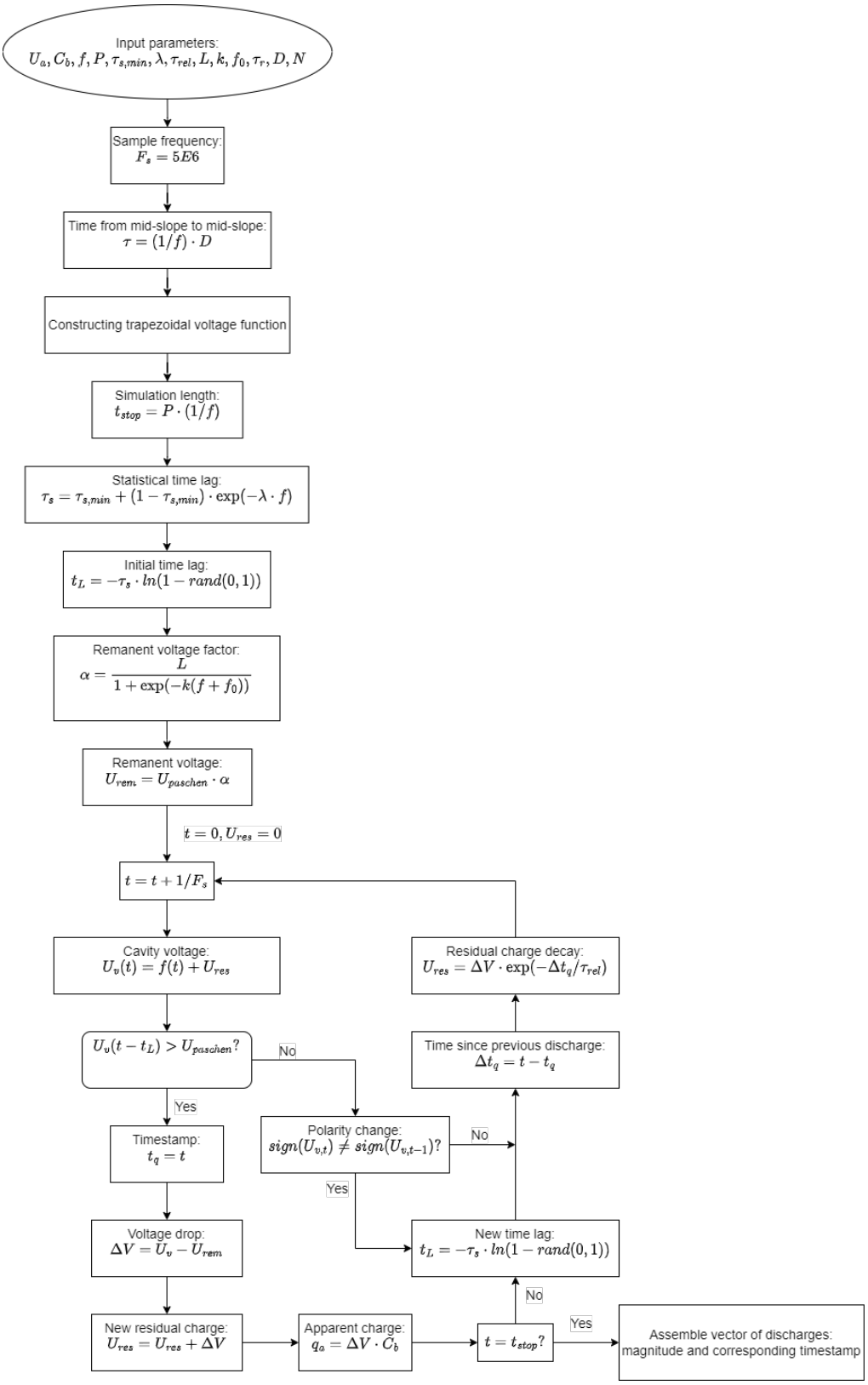

Figure 3.2.2: Flowchart of model with square wave voltage

3.3 Input parameters

With a basis in the capacitive abc model, each element of the dielectric is modelled as a capacitor. However, the three parameters of time lag, charge decay and remanent voltage are implemented and expanded on to understand the impact that each has on the PD behaviour. These parameters are dependent on void surface conductivity and surface emission of electrons, which are known to change with the presence of PD activity [19]. This causes an additional frequency-dependence in PD behaviour as the input parameter values themselves are frequency-dependent.

3.3.1 Constant parameters

The void gap distance d_c, dielectric thickness d_b, material permittivity ϵ_b, and dielectric capacitance C_b are all input parameters that remain constant throughout the simulation. Equation 2.1 is used to find the void voltage corresponding to the applied voltage, and Equation 2.3 is used to find the Paschen voltage for the selected void gap distance.

3.3.2 Voltage function

A list of voltage frequencies is given as an input to allow for a parametric sweep in the desired range. The shape of the applied voltage is implemented in one of two ways; a sine wave or square wave function with frequency and time as input variables. The pre-defined *sin*-function is used for a sine wave voltage. No pre-defined function exists for a square wave voltage that allows for the adjustment of rise time. Such a voltage shape is, in reality, trapezoidal rather than square due to the rise time caused by circuit capacitance. Therefore, a function is created using the Fourier-transform expressed in Equation 3.1. Doing so allows for a free selection of amplitude, rise time, fundamental frequency and duty cycle. Here, τ, τ_r and N are additional input parameters required to calculate the voltage waveform. A higher number of iterations N would lead to a more ideal trapezoidal-shaped function, although it also leads to longer computation time. τ is the time between the mid-points of the flanks, corresponding to the duty cycle, and τ_r is the rise-time. A is the peak-to-peak amplitude, and T_{AC} is the voltage period time.

$$f(t) = A\frac{\tau}{T_{AC}} + 2 \cdot A\frac{\tau}{T_{AC}} \sum_{n=1}^{N} \left[\left(\frac{sin(n\pi f\tau)}{n\pi f\tau} \right) \cdot \left(\frac{sin(n\pi f\tau_r)}{n\pi f\tau_r} \right) \cdot cos(2\pi nft - \pi nf(\tau - \tau_r)) \right] \tag{3.1}$$

A time vector is used as a sweep parameter; each calculation is performed for each step in the time vector. The length of the time-vector is set to $P \cdot T_{AC}$, which is the desired number of voltage cycles times the voltage period. The step-length is given as $1/F_s$ where $F_s = 5E6$, giving a step-length of 200 ns.

3.3.3 Time lag

The time lag is believed to decrease with an increased frequency due to higher availability of free electrons from previous discharges [20]. This is especially true when a very high voltage rate of change is applied, as the voltage would reach the critical Paschen level shortly after a PD event. A stochastic time lag is implemented through an exponential probability distribution per Equation 2.8 with τ_s as the input parameter. R is a function for creating a randomised number between 0 and 1. Each time a discharge occurs, a new time lag is calculated. In addition, a new time lag is calculated each time the polarity of the void voltage changes. This allows for large time lag values relative to the voltage period leading to some half-cycles without any discharge.

A linear relation between τ_s and frequency would quickly lead to very small time lag values. Therefore, an exponential relation is proposed with a maximum value of 1 ms and a minimum value in the region 0.1 - 0.5 ms. At any given frequency, the statistical time lag is calculated using

$$\tau_s(f) = \tau_{s,min} + (1 - \tau_{s,min}) \cdot \exp(-\lambda \cdot f) \tag{3.2}$$

where $\tau_{s,min}$ is the lowest time lag allowed, $(1 - \tau_{s,min})$ gives a vertical shift so that the maximum value of 1 is achieved at f=0, and λ is the decay constant of the time lag. Although the statistical time lag changes with voltage frequency, it remains constant at that given frequency; the statistical time lag in the model does not change depending on overvoltage or time between discharges.

3.3.4 Charge decay

A charge decay is implemented through an exponential decay of the residual voltage between PD events, as per Equation 3.3, with a constant relaxation time constant τ_{rel} [23]. The decay is implemented on the charge left over immediately after the PD event, represented by ΔV. Implementing a charge decay causes a greater frequency-dependence in PD behaviour at lower voltage frequencies where the period is much longer. Further, the effect of charge decay is more significant for sine wave voltage, as a square wave voltage will have a much shorter time between discharges due to the short rise time. In the first time-step, U_{res} is set equal to zero before it is continuously updated inside the feedback loop for each iteration (time-step). The charge decay is assumed to be dependent on material characteristics and not on frequency and voltage rate of change, and is therefore kept constant throughout the simulation.

The exponential decay function used to characterise the charge loss is given in Equation 3.3 [23]

$$U_{res} = \Delta V \cdot exp(-\Delta t_q/\tau_{rel}) \tag{3.3}$$

where Δt_q is the time passed since the PD event.

3.3.5 Remanent voltage

The model is built on the assumption of only Townsend-type discharges and neglects the effects of different discharge types. This means that the remanent voltage is kept at a value close to the critical Paschen voltage. However, as the remanent voltage is affected by the overvoltage at the discharge, it is assumed that an increased voltage rate of change leads to lower remanent voltage due to the larger overvoltage caused by a short rise time. This parameter is also assumed to have a certain frequency-dependency where the discharges become smaller with increased frequency. Due to the time lag becoming relatively larger compared to the voltage period, one should expect fewer and larger discharges to occur. However, due to the increasing remanent voltage with increased frequency, the discharge magnitude will become gradually smaller.

The voltage rate of change- and frequency-dependency of the remanent voltage is implemented using the logistic function in Equation 3.4

$$\alpha(f) = \frac{L}{1 + \exp(-k(f + f_0))} \tag{3.4}$$

where α is the fraction of the Paschen voltage that remains after the discharge, L is the maximum value, k is the growth rate, and f_0 is the mid-point value. The remanent voltage at any given frequency is then found using Equation 3.5

$$U_{rem} = U_{paschen} \cdot \alpha(f) \tag{3.5}$$

By changing L and f_0, the function is shifted vertically and horizontally to allow for different maximum and minimum values, depending on the voltage rate of change.

Chapter 4

Experimental techniques and test procedure

This chapter describes the methodology used in the experimental work. Here, the laboratory setup and test procedures are described in detail. Initial measurements to establish the method's validity are also presented, along with the steps performed in post-processing of the measurement-data.

4.1 Test objects

Test objects were made from resin-rich mica/epoxy/glass-fibre tape (Semicatherm® 366.28-02). The object dimensions were 100 mm × 100 mm × 2 mm, with six tape layers stacked half-overlapping to form a sheet thickness of 1 mm; two cured sheets are pressed together to form one test object with a known void dimension. Voids were created using metal spacers placed on the sheets during the curing process, which was done at 160°C under pressure for one hour. Three test objects were used with three different void gap distances, as shown in Table 4.1.1.

Test object name	**Void diameter**	**Void gap distance**
TO1	20 mm	0.11 mm
TO2	20 mm	0.26 mm
TO3	20 mm	0.52 mm

Table 4.1.1: Test object numbers and void dimensions

Rogowski brass electrodes have been moulded into epoxy [23], and the test object was placed between them. A thin layer of silicone compound was used between the electrodes and the test object to minimise unintended voids. The electrode diameter was 30 mm. Figure 4.1.1 shows an illustration with a void gap distance of 0.5 mm placed in the middle, and Figure 4.1.2 shows a picture of TO3. Due to the void being on one sheet while the other sheet is free for any voids, the position of the voids was not precisely in the middle between the electrodes but rather slightly closer to one electrode. The material and setup parameters are listed in Table 4.1.2.

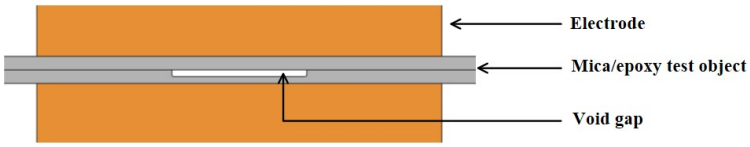

Figure 4.1.1: Sketch of test object with 0.5 mm void gap distance

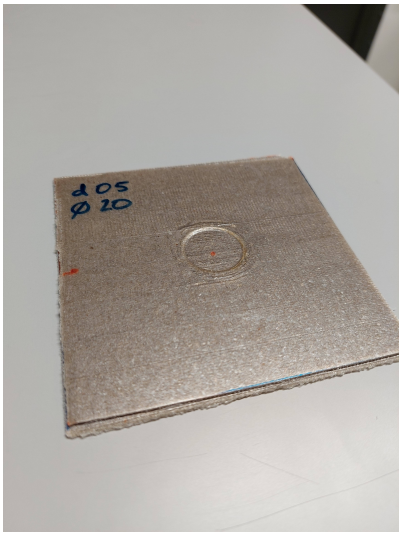

Figure 4.1.2: Picture of test object with 0.52 mm void intrusion

Parameter name	**Symbol**	**Value**	**Unit**
Test object thickness	d_a	2	mm
Electrode diameter	D_{el}	30	mm
Mica/epoxy permittivity	ϵ_b	3.94	1
Void air permittivity	ϵ_c	1	1

Table 4.1.2: Test object parameters and material properties

4.2 Laboratory setup

The applied voltage was generated using a signal generator connected to an HV power amplifier. A high-voltage probe was used to measure the voltage. Figure 4.2.1 shows a circuit diagram of the laboratory setup, while Figure 4.2.2 shows a picture of the test object when connected to the electrodes, and Figure 4.2.3 shows a picture of the laboratory setup. A capacitor was placed in parallel with the test object to set the rise time when applying square wave voltages. Three setups were used; no parallel capacitor (shortest rise time), 300 pF, and 1 nF. The applied voltage and PD voltages were measured using an oscilloscope connected to a high-frequency current transformer (HFCT) around the ground cable attached to the test object. The signal generator and the oscilloscope was controlled using a PC, as described in section 4.4.

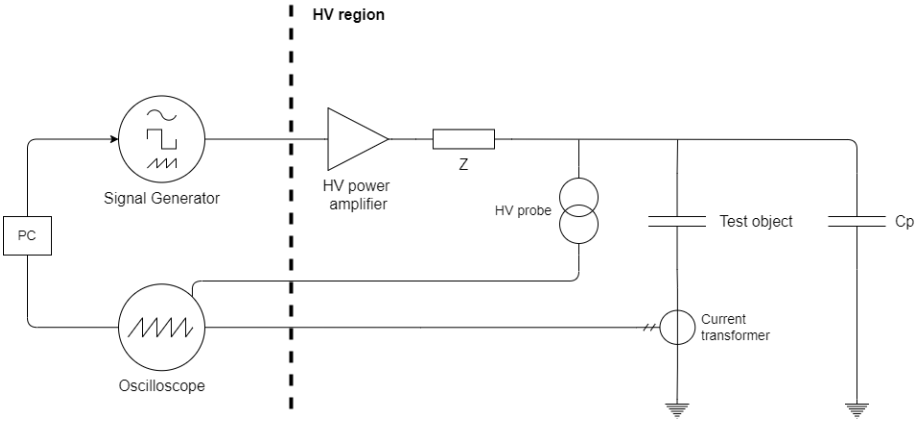

Figure 4.2.1: Schematic of PD test setup

The specific equipment that was used in the setup is listed below:

- Agilent 34972A, signal generator
- North Start High Voltage PVM-4-2, high-voltage probe
- Tektronix DPO5104, oscilloscope
- MagneLab CT-B0.25-B, Current transformer

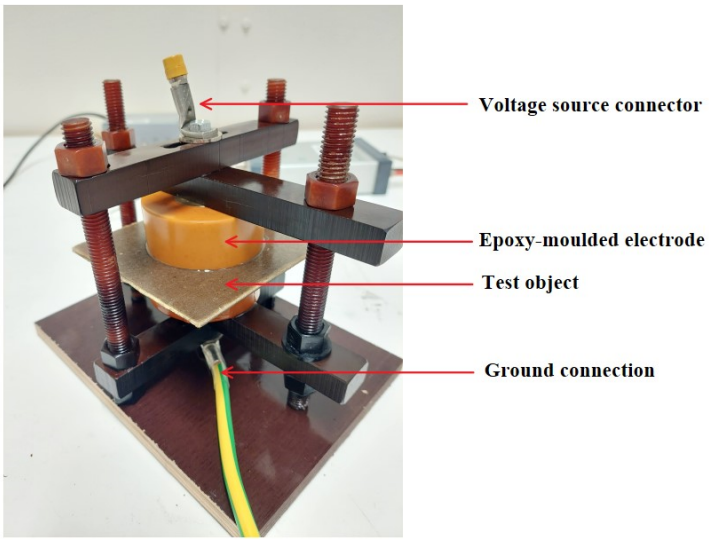

Figure 4.2.2: Picture of test object connected to fastener

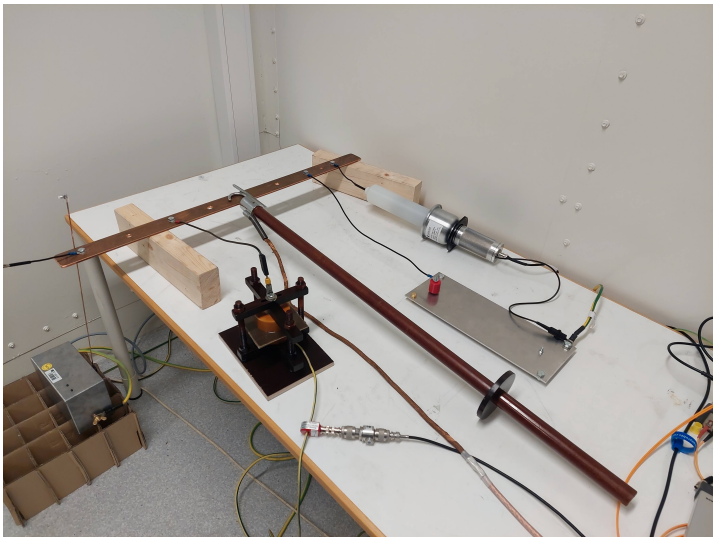

Figure 4.2.3: Picture of the laboratory setup

Due to the high voltage frequencies investigated in this project, standardised testing equipment was not available for use. For this reason, using an oscilloscope and an HFCT represented the most feasible way. Firstly, the standardised testing equipment available, Omicron MPD 600, did not support voltage-frequencies above 2.1 kHz. Secondly, when using the MPD 600 equipment, a coupling capacitor with significantly larger capacitance than the test object is desired [24]. This leads to a high circuit capacitance, thereby limiting the voltage rise time. Therefore, to investigate higher voltage frequencies and square wave voltage with more than 35 $V/\mu s$ rate of change, measurements had to be done using non-standardised equipment. However, an initial measurement was done with the MPD 600 system to compare and calibrate the HFCT measurements. From this comparison, the validity of the measurements can be considered.

The two PD parameters of interest were the discharge repetition rate and the discharge magnitude. The measurement settings used with the oscilloscope were chosen carefully, with some clear advantages and shortcomings. The repetition rate was measured using the *peak detection* mode on the oscilloscope over a time period corresponding to 500 voltage cycles for each frequency. In the case of repetition rate, it was sufficient to register the presence of such a pulse; one does not need to know the discharge magnitude to register the PD's time-stamp. Therefore, it was not necessary to investigate each pulse in high-resolution detail. The *peak detection* mode could then be used with a resolution (i.e. time-step) of 1μs to register the peak of each pulse. The maximum recording length possible on the oscilloscope is limited by the size of the data file, which is proportional to the resolution of the recording. Consequently, it was preferable to have as low resolution as possible to measure a large number of voltage periods, thereby obtaining an acceptable data sample size. As a pulse duration is usually in the range of a few hundred nanoseconds [15], a 1 μs time-step was deemed appropriate. A much smaller time step would lead to multiple peaks of the same pulse being registered, thus giving the impression that multiple discharges occur close to each other when they are, in fact, only one discharge. A much longer time-step would increase the chance of the opposite, namely registering separate discharges as the same one, storing only one of multiple discharges.

Using an oscilloscope to analyse discharge magnitude proved significantly more challenging. Standardised testing equipment like the Omicron MPD 600 system uses a method of pulse integration to calculate the apparent charge of the PD, described in Equation 4.1.

$$q_a = \frac{1}{R} \cdot \int_{t1}^{t2} u(t)dt \tag{4.1}$$

To obtain a valid answer using this method, one requires a high-resolution measurement of the PD pulse and excellent noise reduction. The calculated integral, corresponding to the PD current, is proportional to the apparent charge of the PD. The immediate issue that arose was how the oscilloscope registers and stores data. The oscilloscope registers all data, including the noise between discharges, and stores it in one file. Using a sampling frequency of 200 MS/s, equal to a 5 ns resolution, and measuring over a time period of 50 ms (5 voltage periods at 100 Hz), the number of stored data-points is 10M. The upper limit of data-points supported by this oscilloscope is 25M, meaning that any analysis of discharge magnitude at a given frequency will be based on a limited amount of voltage cycles. It is possible to collect data from more voltage periods at higher voltage frequencies, though it is still a minimal amount.

4.3 Measurement verification

An initial comparison had to be done with the Omicron MPD 600 system to evaluate the validity of the HFCT measurements. In addition to validating the PDIV for each test object, a reference point for the apparent charge had to be established due to the HFCT measuring voltage and not charge. In addition, post-treatment of the HFCT measurements was necessary to distinguish between discharges and noise.

4.3.1 Partial discharge detection

The PD activity was recorded with MPD 600 to establish phase-resolved partial discharge (PRPD) plots at multiple frequencies. A PRPD plot shows all the discharges superimposed on a single voltage cycle, thereby giving the phase position of the discharges. Although the use of MPD 600 was limited to frequencies below 1.5 kHz due to the large capacitance of the circuit, measurements at lower frequencies show a high degree of similarity between the two, as shown in Figure 4.3.1 and

Figure 4.3.2. It should be mentioned that the MPD 600 recording was done over a set time period of 10 s, while the HFCT measurement was done for 500 voltage cycles at each frequency. This leads to a much higher number of discharges on the MPD 600 recording, but a general pattern is still clearly visible. The MPD 600 recording also shows that the discharge magnitudes are in the order of 100 pC to 1 nC. The HFCT measurement does not, as mentioned, show the discharge magnitudes but rather the peak value of the discharge pulses. The discharge voltage pulse does not directly translate to discharge magnitude, even though a higher pulse magnitude generally indicates a larger discharge magnitude. From this, it was assumed that measurements using the HFCT and oscilloscope are valid for detecting the presence of PDs.

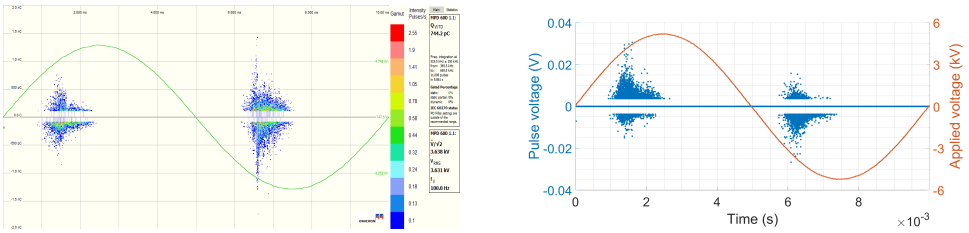

(a) MPD 600 (b) HFCT

Figure 4.3.1: PRPD plot, TO3 at 100 Hz sine voltage

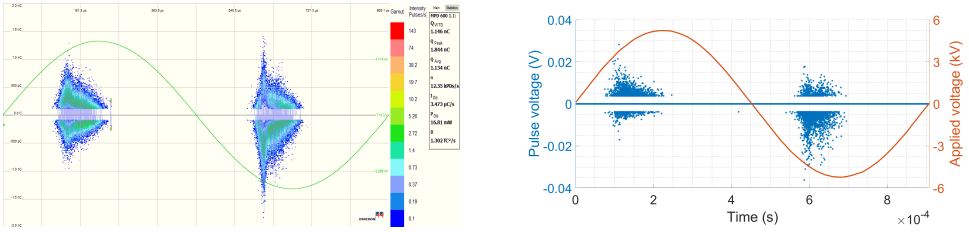

(a) MPD 600 (b) HFCT

Figure 4.3.2: PRPD plot, TO3 at 1100 Hz sine voltage

It should be noted that, in reality, the discharges are not bipolar in a given half-period. This means that in each half-period, there will only be discharges with either negative or positive polarity, not both. It appears so from the PRPD plots due to misinterpretation in the measurement system caused by oscillations in the PD pulses. Further, the polarity when using the HFCT is also affected by the direction in which it is connected to the wire.

4.3.2 Noise filtering

The raw data from HFCT measurements contain a significant amount of noise. This noise is easily distinguished from the PDs due to the significant differences in amplitude. However, to integrate the voltage pulse, the noise must be removed to avoid a continuous increase or decrease between the PD pulses. This is done in two steps; a digital highpass filter is applied to remove any offset caused by the circuit capacitance, and a threshold value is set to remove all values close to zero. Figure 4.3.3 shows an example of how the signal ends up after this process. Even though this is somewhat sufficient, some information is lost due to the voltage pulse also containing small values below the threshold value, which are set to zero. This is limited to a certain extent by implementing a requirement that multiple consecutive values must be below the threshold value, and not just one single data-point.

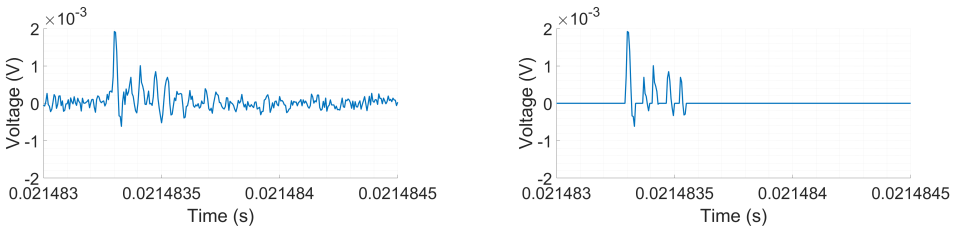

(a) Unfiltered (b) Filtered

Figure 4.3.3: PD voltage pulse, TO3 at 100 Hz sinusoidal voltage

The filtered signal is run through a cumulative integration function to obtain the discharge current as shown in Figure 4.3.4, and the average value is found by calculating the average current in each half-period, i.e. the absolute values of the change in current magnitude in each half-period.

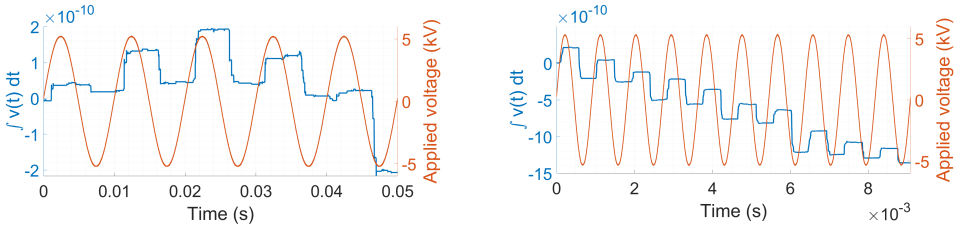

(a) 100 Hz (b) 1100 Hz

Figure 4.3.4: Cumulative integration of PD pulse voltage

4.4 Test procedure

The test sequence was run automatically by programming the function generator and oscilloscope to apply the correct frequency and conditioning time. For each test object, the PDIV was found by gradually increasing the applied voltage amplitude until sustained discharges occurred, as illustrated in Figure 4.4.1. The voltage was increased in steps of 80 V and held for 10 s until PD activity was observed. When PDs were observed, the applied voltage was maintained for a minimum of 2 min to confirm sustained PD activity. If the PD activity stopped, the sequence was continued in the same way. This procedure was done with 50 Hz sinusoidal voltage to verify the presence of discharges using the Omicron MPD 600 system.

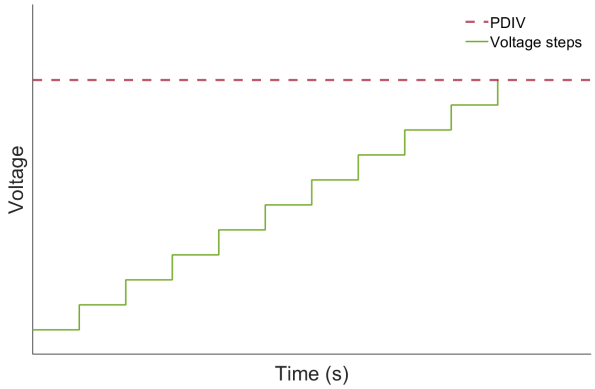

Figure 4.4.1: PDIV test sequence

The test sequence was performed at a constant voltage 10% above the PDIV. An initial conditioning at 50 Hz sinusoidal voltage for 5 min was done to assure that the conditions were the same each time the test sequence was run. An intermediate conditioning of 90 s at each test frequency was performed before each measurement to reduce the memory-effects of the previous frequency, which would have been more significant if no intermediate conditioning was performed. The subsequent frequency was then applied, as illustrated in Figure 4.4.2.

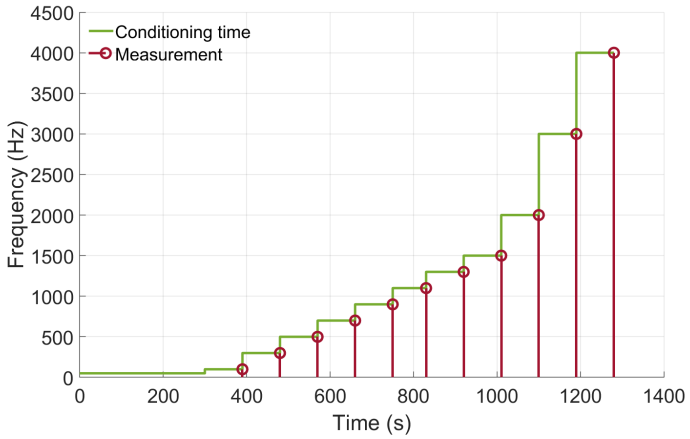

Figure 4.4.2: Frequency application procedure in laboratory

The same test sequence was repeated for all applied voltage shapes and test objects. Four voltage shapes were used; sine wave and square wave with three different rise times. The square wave voltages' rise time was adjusted by switching the parallel capacitor in the circuit. Table 4.4.1 summarises the investigated rise times with the corresponding voltage rates of change. The rise time was measured on the oscilloscope, measured as the time from 10% amplitude to 90% amplitude of the rising voltage flank. The numbers given in Table 4.4.1 are calculated to show the rise time from 0% to 100%, which is the input used to calculate the square wave function as explained in subsection 3.3.2. The original measurements are given in Appendix B.

Parallel capacitance	**Rise time**	**Voltage rate of change**
1 nF	280 μs	35 V/μs
300 pF	70 μs	130 V/μs
0 F	30 μs	300 V/μs

Table 4.4.1: Parallel capacitance values with corresponding rise time and voltage rate of change

Chapter 5

Results and discussion

This chapter presents and analyses the experimental results from laboratory measurements and model simulations. Results showing the PDIV, discharge distribution, PD repetition rate and PD magnitude are all presented in turn. Important observations are briefly discussed throughout the chapter as the various results are presented, with a more comprehensive discussion at the end.

5.1 Model input parameter values

The model input parameters U_{rem}, τ_s and τ_{rel} are estimated through a comparison with the experimental results. As the largest data sample was achieved on the number of discharges, the process of selecting the parameter values started with adjusting the input parameters to obtain a result similar to the measured PD repetition rate. Here, the statistical time lag had the greatest impact. Then, the parameters were adjusted further, emphasising the remanent voltage and charge decay to obtain model results on PD magnitude that were similar to the measured results.

The selected values used in Equation 3.2, Equation 3.3 and Equation 3.4 are listed in Table 5.1.1. The impact of various parameter values is explained in more detail in Appendix A.

Parameter \ Voltage	Sine	35 V/μs	130 V/μs	300 V/μs
L	0.95	0.95	0.95	0.95
k	1.5E-3	5E-3	5E-3	5E-3
f_0	2500	400	250	150
τ_{rel}	0.01	0.01	0.01	0.01
λ	0.8E-3	1E-3	3E-3	5E-3
$\tau_{s,min}$	0.25E-3	0.35E-3	0.25E-3	0.15E-3

Table 5.1.1: Model input parameter values

Figure 5.1.1 shows the suggested frequency-dependent behaviour of the statistical time lag for each applied voltage, where a larger voltage rate of change leads to a faster drop in τ_s and a lower minimum value.

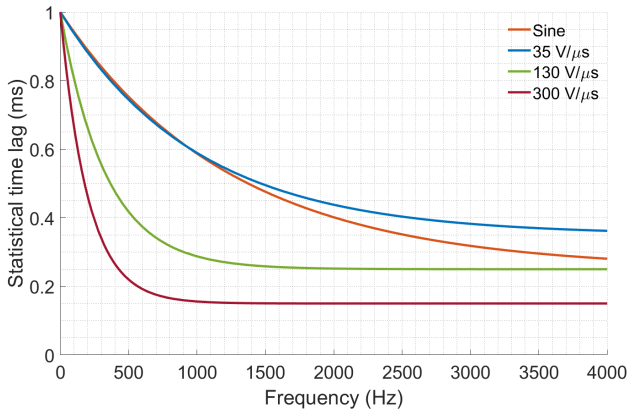

Figure 5.1.1: Frequency-dependent time lag for different voltage dV/dt

Figure 5.1.2 shows the suggested frequency-dependent behaviour of α for each applied voltage with the selected input parameters. At a higher voltage rate of change, the α function is shifted to allow for a larger discharge.

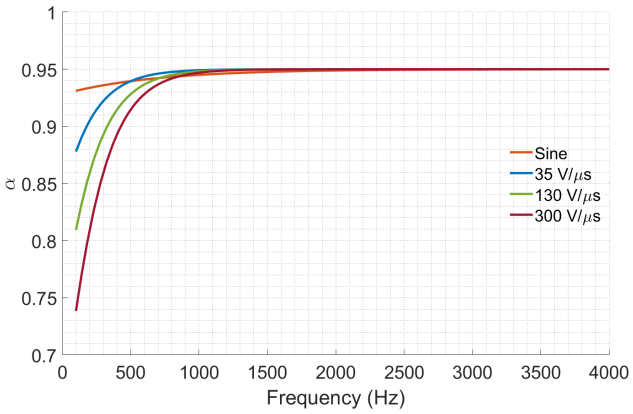

Figure 5.1.2: Proportion of $U_{paschen}$ remaining after a PD event

5.2 Inception voltage

The method for finding the PDIV was described in section 4.4. Table 5.2.1 lists the expected and measured PDIV values for the three test objects. The measured PDIV was found to be close to the predicted values in TO2 and TO3, while in TO1 the difference was larger.

Test object	Void gap distance	Model PDIV	Measured PDIV
TO1	0.11 mm	5.20 kVp	4.92 kVp
TO2	0.26 mm	4.62 kVp	4.68 kVp
TO3	0.52 mm	4.81 kVp	4.73 kVp

Table 5.2.1: Expected and measured PDIV values

In addition to this substantial difference in PDIV, further measurements on TO1 indicated that the discharges present were of such a low magnitude and repetition rate that it was not possible to separate it from noise in an efficient way. Possible explanations for both the difference in PDIV and the lower PD magnitude are likely related to defects and imperfections in the void. A very small metal spacer had to be used for the small void gap distance, and it is likely that the void was not perfectly cylindrical and therefore a much less homogeneous field distribution.

Therefore, TO1 had to be removed from the investigated sample of test objects and will not be included further. Appendix B shows a selection of measurement results from TO1 to justify its exclusion.

5.3 Distribution of discharges

The distribution of PDs given by a model simulation is shown by PRPD plots in at Figure 5.3.1, showing both 100 Hz and 2000 Hz sine wave voltage. The impact of statistical time lag is shown through a change in the number of discharges, where an increasing frequency leads to significantly fewer discharges. Although difficult to see, at 100 Hz the density of discharges is greater early in the phase. Even though the statistical time lag is decreased with increasing frequency, the decrease in voltage period is far greater, leading to fewer discharges per voltage period.

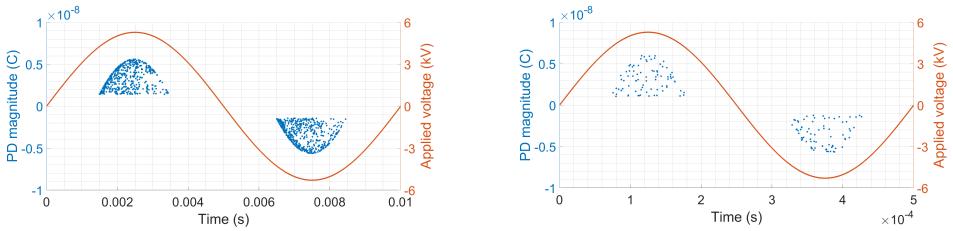

(a) 100 Hz (b) 2000 Hz

Figure 5.3.1: PRPD plot from model, TO3 with sinusoidal voltage

Figure 5.3.2 and Figure 5.3.3 compares the measurements with model simulations when a square wave voltage with rise time of 70 μs is applied. A clear difference is observed in the phase position of the discharges; in the measured results, the discharges only occur in the section of the period where the voltage is rising or falling, while in the model results, there is a far greater spread in phase position. The measurement results show that using square wave voltage with a set rise time is helpful to investigate the impacts of voltage frequency and voltage rate of change, as only the frequency is changed. By maintaining the same voltage rate of change and voltage peak level, an increased frequency will lead to a greater spread in phase position as the rise time makes out a more significant section relative to the period time. Still, the PDs only occur during the rise and fall section of the voltage.

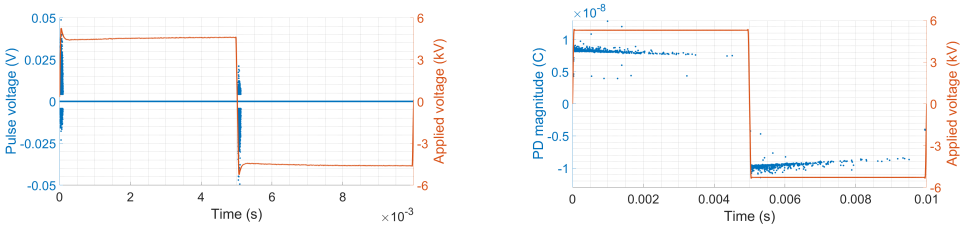

(a) Measurement (b) Simulation

Figure 5.3.2: PRPD plot, TO3 with trapezoidal voltage at 100 Hz with rise time of 70 μs

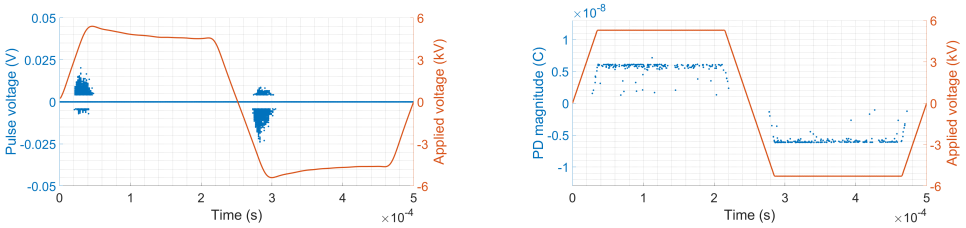

(a) Measurement (b) Simulation

Figure 5.3.3: PRPD plot, TO3 with trapezoidal voltage at 2000 Hz with rise time of 70 μs

A more similar result could have been achieved if the statistical time lag was reduced, although this would have led to a close-to-zero difference in the number of discharges. As will be shown in section 5.4, this is not the case; the number of discharges drastically reduces at increased voltage frequencies.

5.4 Repetition rate

First, the measured PD repetition rate is presented before a comparison with the model simulation results.

5.4.1 Experimental measurements

The discharge repetition rate is measured as described in section 4.4 and presented in the form of *discharges per voltage period* rather than the more conventional *discharges per second* to give a greater insight into the effects of changing voltage parameters.

The experimental results are shown in Figure 5.4.1 and Figure 5.4.2. The measured repetition rate decreases with an increasing voltage frequency; a greater voltage rate of change is seen to give a greater decrease in repetition rate. When sine wave voltage is applied, an initial increase in repetition rate is followed by a decrease until the frequency is about 1500 Hz. As the frequency continues to increase, the repetition rate remains relatively constant in TO2 while it slightly increases in TO3. When square wave voltages are applied, the repetition rates at low frequencies are significantly higher than with sinusoidal voltage. Rather surprisingly, the highest repetition rate is measured when a voltage rate of change of 130 V/μs is applied, followed by 35 V/μs and 300 V/μs in decreasing order. Looking at Figure 5.4.2, the fast decline in repetition rate with 35 V/μs means that it falls below the line of 300 V/μs at 300 Hz and below the sine-line at 900 Hz. If the voltage rate of change governs the repetition rate at a given frequency, one might expect the highest repetition rate when 300 V/μs is applied rather than 130 V/μs.

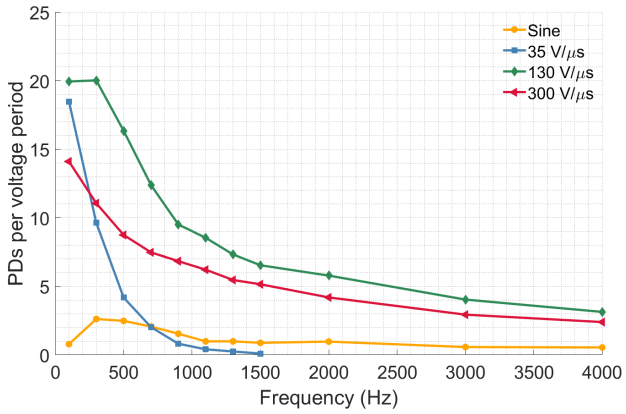

Figure 5.4.1: TO2, number of discharges per voltage period

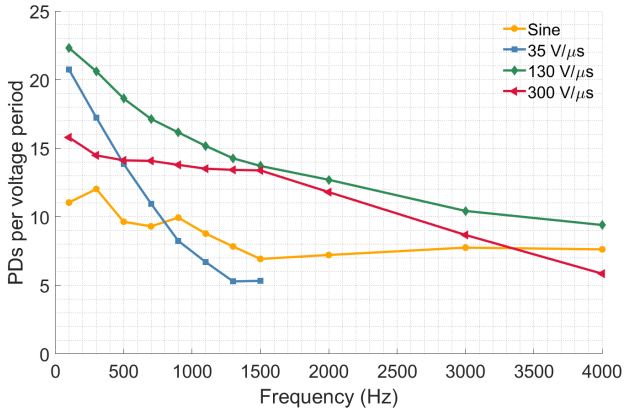

Figure 5.4.2: TO3, number of discharges per voltage period

The same behaviour is observed in both test objects; an increasing square wave voltage frequency leads to a lower repetition rate, and the voltage rate of change affects the numerical value of the repetition rate as well as the slope, i.e. the rate of change in repetition rate when frequency is increased. From these measurements, it can be speculated that the PD repetition rate increases with an increased voltage rate of change up to a certain value before it decreases, which may be due to a change in other parameters such as discharge type and charge decay mechanisms.

Further, it is observed that when a square wave voltage is applied, the discharge repetition rate at 100 Hz is in the region of 15 to 20 discharges per voltage period in both test objects. At a given voltage rate of change, there is a small difference in the two test objects at 100 Hz, but as frequency increases, so does the difference in repetition rate. When a sinusoidal voltage is applied, a significant difference between the two test objects is observed at all frequencies.

The rates of decline in discharge repetition rate are given in Table 5.4.1, calculated from the measurements done in the frequency range of 100 to 1500 Hz at regular steps in voltage frequency of 200 Hz. As an example, this shows that on average, the PD repetition rate decreases by 52.1% every 200 Hz when 35 V/μs is applied to TO2, while in TO3 it decreases by 17.3% every 200 Hz. From this, a large geometry-dependence can be assumed, meaning that the field distribution and void capacitance affect the rate at which the repetition rate declines with increasing frequency.

Voltage rate of change	**Decline rate, TO2**	**Decline rate, TO3**
35 V/μs	52.1%	17.3%
130 V/μs	14.4%	6.7%
300 V/μs	13.2%	2.3%

Table 5.4.1: Average decline in discharge repetition rate per frequency step (200 Hz) in the range 100 - 1500 Hz

5.4.2 Comparison with model results

The results of the simulated discharge rate are compared with the measured results and shown in Figure 5.4.4. Due to the large difference in numerical values, the simulated results are plotted against the left y-axis, and the measured results are plotted against the right y-axis, with a factor 10 difference between the two axes. The simulation results are shown with solid lines, while the measured results are shown with dotted lines.

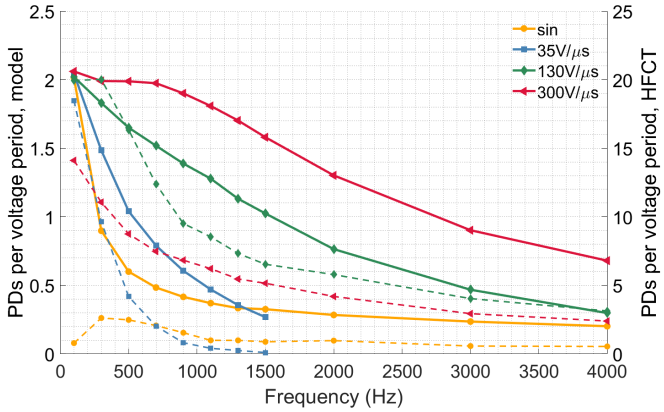

Figure 5.4.3: TO2, comparison of simulated and measured discharge rate per voltage period

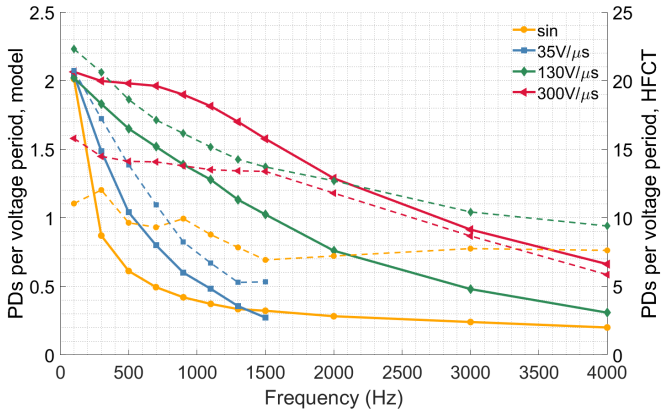

Figure 5.4.4: TO3, comparison of simulated and measured discharge rate per voltage period

Several differences in behaviour are observed. Firstly, the mentioned difference in numerical value is significant between the simulations and measurements. Secondly, the simulated discharge rate is the same at 100 Hz for all applied voltages, while the measured results shows a larger difference between the applied voltages at 100 Hz. Thirdly, the simulated discharge rate with sine wave voltage drops quickly between 100 Hz and 500 Hz, while the measured results indicates a much lower drop in repetition rate; an initial increase from 100 Hz to 300 Hz can even be observed.

Some similarities are also observed. Even though there is a difference in numerical value, the general behaviour is the same; an increasing frequency leads to a decrease in discharge rate. This indicates that using frequency-dependent input parameters goes some way in predicting the general behaviour of the discharge rate. A more careful selection of input parameter values should give a relative change much closer to the measured results.

A particularly important observation is that there is no difference in model PD repetition rate between the two test objects, neither in the numerical values nor the rate of decrease with increasing frequency, as shown in Table 5.4.2 and Table 5.4.3. Considering that the void capacitance C_b does not affect the statistical time lag, charge decay or remanent voltage in the model, this is as expected. However, we do observe a difference in the measured discharge rates in the two test objects, thereby showing a clear limitation in the model. It can also be seen that there is a much larger difference between the model simulation and measurements in TO2 than in TO3.

Voltage rate of change	Decline rate, model	Decline rate, measured
35 V/μs	25.2%	52.1%
130 V/μs	9.3%	14.4%
300 V/μs	3.7%	13.2%

Table 5.4.2: Average decline in discharge repetition rate per frequency step (200 Hz) in the range 100 - 1500 Hz, in TO2

Voltage rate of change	Decline rate, model	Decline rate, measured
35 V/μs	25.0%	17.3%
130 V/μs	9.3%	6.7%
300 V/μs	3.8%	2.3%

Table 5.4.3: Average decline in discharge repetition rate per frequency step (200 Hz) in the range 100 - 1500 Hz, in TO3

Comparisons of the measured results with other experiments should be made with great care, as there is often a significant difference in the types of voids, dielectric material, voltage amplitudes and measurement techniques used. That being said, experimental measurements from Gäfvert *et al.* [17] showed that the PD repetition rate per voltage period was reduced dramatically, from 800 to 400 PDs per voltage period, as the frequency was increased from 10 Hz to 100 Hz sinusoidal voltage at 9 kV rms. Their model results when statistical time lag was taken into account predicted no drop in repetition rate in that frequency range, and a drop from 12 to ~ 8 PDs per voltage period as the frequency was increased from 100 Hz to 1000 Hz. The difference was mainly explained through the fact that the test objects contain several voids of various types. They concluded that qualitatively, the modelling could be used to interpret the frequency-dependency of PD patterns, as a clear statistical effect was shown when the frequency was increased above 100 Hz. This shows that significant differences in numerical values when comparing measurements with models are expected, as the model is idealised to the extent that there is a significantly different outcome.

5.5 Discharge magnitude

First, the measured PD magnitudes are presented before a comparison with the model simulation results is presented.

5.5.1 Experimental measurements

As explained, it was sufficient to measure the PD voltage pulse and integrate it to explain the behaviour in PD magnitude. However, in order to evaluate to validity of the measurement, it is helpful to estimate the corresponding charge of the voltage integral. Therefore, the average discharge magnitude was first measured using the Omicron MPD 600 up to 1500 Hz, then compared with a simultaneous measurement using the HFCT. The HFCT measurement was post-treated as described in subsection 4.3.2. The resulting apparent charge and discharge current is shown in Figure 5.5.1 and Figure 5.5.2 for TO2 and TO3 respectively. It should be noted that the HFCT discharge current measurement is plotted against the left y-axis, and the MPD 600 apparent charge measurement is plotted against the right y-axis due to the difference in numerical values. This shows that although the behaviour is similar for the two, the values are different.

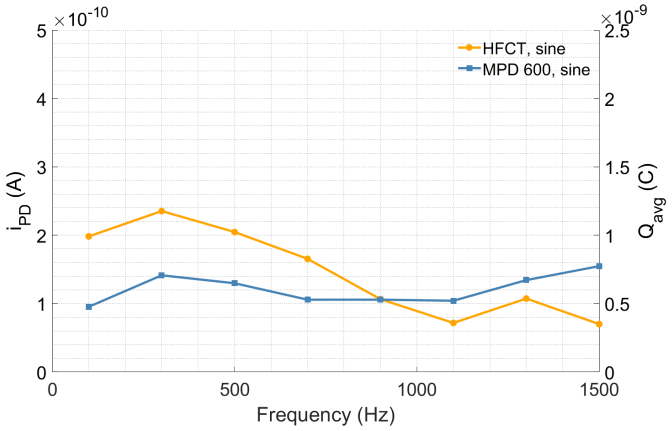

Figure 5.5.1: Apparent charge, TO2 with Omicron MPD 600

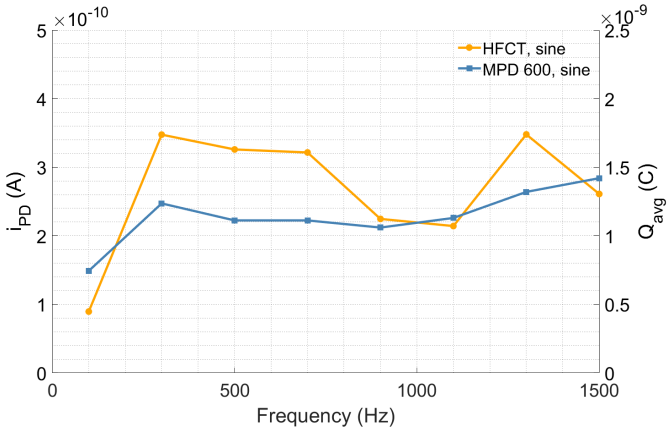

Figure 5.5.2: Apparent charge, TO3 with Omicron MPD 600

The void resistance R is equal to the fraction between the current and charge at any given frequency, as shown in Equation 4.1. An effort was made to estimate R through the fraction between the HFCT and MPD 600 measurement, and is shown in Table 5.5.1. It should be stressed that there is considerable uncertainty in the values due to the lack of data in the HFCT measurement, shown by the maximum and minimum values compared to the mean.

	TO2	**TO3**
Max R	0.416 Ω	0.293 Ω
Min R	0.091 Ω	0.120 Ω
Mean R	0.246 Ω	0.229 Ω

Table 5.5.1: Fraction between voltage integral and apparent charge, corresponding to void resistance R

Having established a relation between the HFCT voltage measurements and the MPD 600 apparent charge, further measurements are performed with square wave voltages. The results for TO2 and TO3 with all voltages are shown in Figure 5.5.3 and Figure 5.5.4 respectively. The discharge current is observed to decrease with increasing frequency when square wave voltages are applied; a relatively large decrease in discharge current occurs with increasing frequency until 1500 Hz, followed by a slow decrease at higher frequencies. Larger discharge currents are measured across all frequencies when a greater voltage rate of change is applied. Comparing the two test objects, larger values for discharge current, and thereby discharge magnitude, are observed in TO3. This is also as expected due to the larger void capacitance of TO3, which has a larger void gap distance as per Equation 2.11 and Equation 2.12.

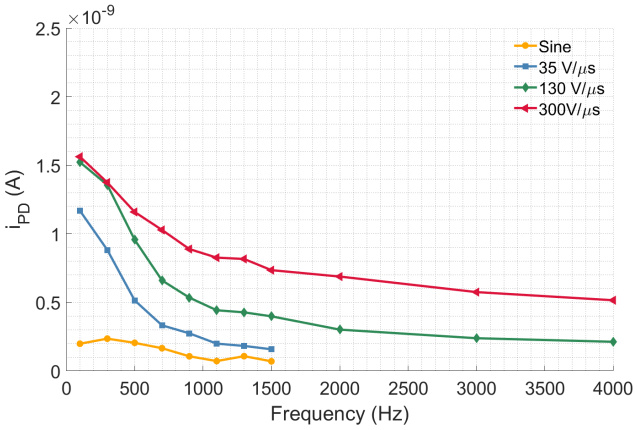

Figure 5.5.3: Voltage pulse integral, TO2 with HFCT measurements

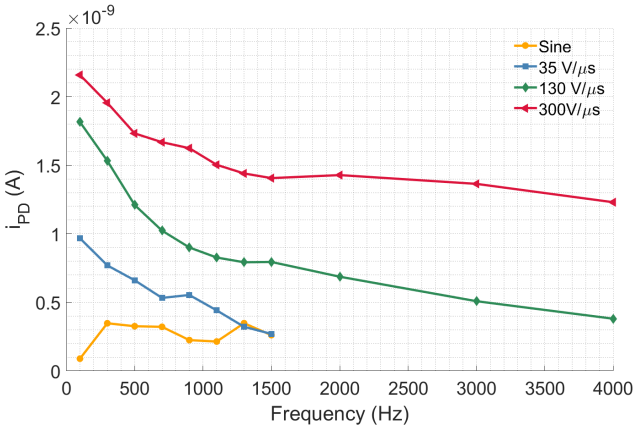

Figure 5.5.4: Voltage pulse integral, TO3 with HFCT measurements

The decline rates in discharge current are similar in the two test objects, as shown in Table 5.5.2. Looking at the square wave voltages, the lowest voltage rate of change (35 V/μs) has the greatest average decline in discharge current when frequency is increased. In both test objects, it is observed that the decline rate in discharge current becomes lower when the voltage rate of change increases, indicating a correlation between the voltage rate of change and the PD magnitudes' frequency-dependence.

Voltage rate of change	**TO2**	**TO3**
35 V/μs	24.1%	16.2%
130 V/μs	16.8%	10.9%
300 V/μs	10.1%	5.9%

Table 5.5.2: Average decline in discharge current per frequency step (200 Hz) in the range 100 - 1500 Hz

Evaluating these results, it is as expected that the square wave voltages give a significantly higher discharge magnitude than sine wave voltage due to the rapid increase in voltage. With a given time lag, the voltage magnitude will have increased much more with a square wave voltage than a sine wave, leading to much higher discharge magnitudes. For a sine wave voltage, a relatively large variance in discharge magnitude is also expected since the time lag has a greater effect on magnitude when the voltage is continuously changing, compared with a square wave voltage that quickly reaches its maximum value where it remains for a longer period of time.

5.5.2 Comparison with model results

Figure 5.5.5 and Figure 5.5.6 shows the results of the simulated discharge magnitudes compared with the measured values. Here, Equation 4.1 is applied with the mean values of R from Table 5.5.1 to better compare the numerical values. The model simulation results are given in solid lines, and the measured values are given in dotted lines.

With the selected parameter input values to the model, a lower voltage rate of change gives both a lower discharge magnitude and a slower decrease in discharge magnitude with increasing frequency.

Comparing the simulated and measured results, it is clear that the simulated discharge magnitudes are larger than the measured ones. This is most evident with sine wave voltage and square wave voltage with a low voltage rate of change. On the other hand, when the highest voltage rate of change is applied, the simulated and measured discharge magnitudes are numerically much closer.

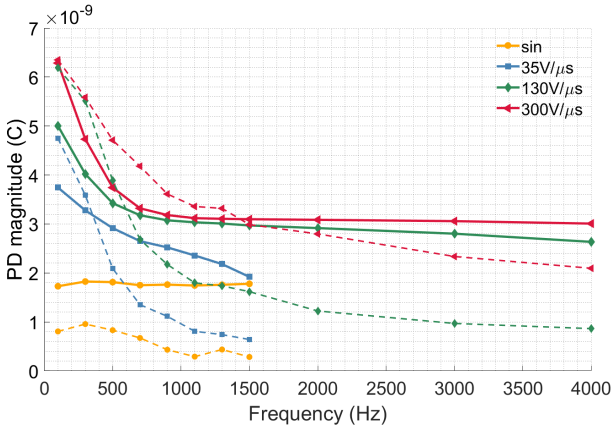

Figure 5.5.5: TO2, average discharge magnitude. Simulated results are given in solid lines and measured results are given in dotted lines.

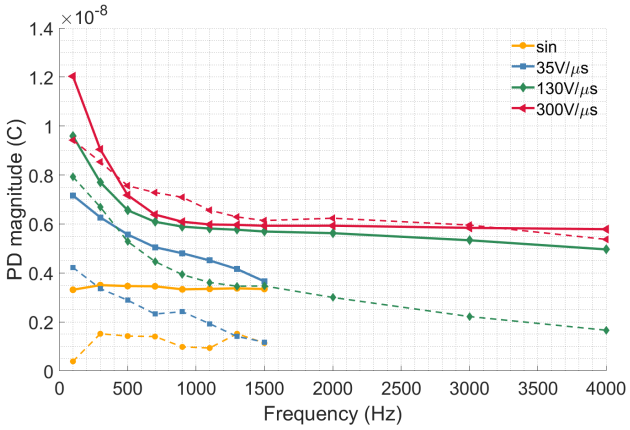

Figure 5.5.6: TO3, average discharge magnitude. Simulated results are given in solid lines and measured results are given in dotted lines.

The simulation results of the two test objects are numerically different but have the same rates of decline, as shown in Table 5.5.3 and Table 5.5.4. As the void capacitance C_b is multiplied with the voltage drop to obtain the discharge magnitude, a different void capacitance is expected to lead to a different magnitude but the same behaviour. This does not fit with the measured results, which show a clear dependency on both voltage rate of change and void geometry.

Voltage rate of change	**Decline rate, model**	**Decline rate, measured**
35 V/μs	9.06%	24.1%
130 V/μs	6.91%	16.8%
300 V/μs	9.11%	10.1%

Table 5.5.3: Average decline in discharge current per frequency step (200 Hz) in the range 100 - 1500 Hz, in TO2

Voltage rate of change	**Decline rate, model**	**Decline rate, measured**
35 V/μs	9.13%	16.2%
130 V/μs	6.91%	10.9%
300 V/μs	9.11%	5.9%

Table 5.5.4: Average decline in discharge current per frequency step (200 Hz) in the range 100 - 1500 Hz, in TO3

Comparison with other works can again be made with care, as no other works have been found that directly compare discharge magnitude with voltage frequencies above 100 Hz. Forssén and Edin [20] used a similar approach as in this thesis,

where model input parameter values were selected to give the closest results to the measurements. Their measurements showed a decrease in discharge magnitude with increased voltage frequency from 1 Hz to 100 Hz sinusoidal voltage. Further, they found that as the voltage frequency was increased, the statistical time lag had to be reduced, from 10 ms at 10 Hz to 2 ms at 100 Hz, to achieve a similar number of discharges, discharge magnitude and spread in PD phase position as measured experimentally. They concluded that there was a radical change in cavity surface properties which was probably due to the short time between consecutive PDs. They also conclude that a transition in discharge type can occur due to the change in number of electrons in shallow traps in the void, which may be part of the explanation for why the statistical time lag and surface conductivity changes with increasing frequency [20].

5.6 Evaluation

Comparing the experimental results with the simulated results, a significant difference in the numerical values, as well as some difference in the PD behaviour, is found. The suggested exponential relations of statistical time lag and remanent voltage with frequency go some way in predicting the behaviour at increasing frequencies, indicating that these parameters need to be modelled with a frequency dependence. However, as shown from the PRPD plots there is a much larger spread in the simulated results than what the measurements show. The small spread in phase position of the measured PDs indicates that the time lag remains relatively small compared to the voltage period, even at higher frequencies. However, if this is implemented in the model then the number of discharges would not decrease. We may therefore speculate that a change in the discharge type leads to a shorter time between discharges and a short time lag, while also decreasing the total number of discharges as voltage frequency increases.

The specific values chosen for these parameters are not necessarily the most interesting aspect and should be regarded more as examples than assertions. The interesting aspect is general behaviour with changing voltage frequency and how the various ways of modelling these parameters affect the overall results of the simulation.

The limitations of this model, and the way in which the parameter values were chosen, become most evident when applying a sinusoidal voltage to the model. As a sinusoidal voltage changes both the voltage period and voltage rate of change when the frequency is increased, the result relies on a correct understanding of how the input parameters change. If either the frequency dependence or the voltage rate of change dependence is not modelled correctly, the overall result will not be correct.

Comparisons with other works show that a certain difference in measured results and model predictions is to be expected, and various hardly-achievable parameters likely play a part in this. In this thesis, a change in void surface properties and discharge type is only accounted for to a limited extent in the form of charge decay and a change in remanent voltage. More detailed modelling of these, where the charge decay rate is not constant and discharges with much larger magnitudes and areas are included, may improve the model substantially. The problem of an inductive research approach is that it does not necessarily give a thorough understanding of the physics behind the phenomenon, especially if there is a limited amount of empirical data available. One may be able to extract qualitative

descriptions of the behaviour, but quantitatively there is not enough empirical data to draw any theoretical conclusions from.

5.7 Sources of error

Numerous sources of error may explain both the difference in numerical values and frequency behaviour of the model results, as well as the validity of the experimental results themselves. As the model's development is partly based on existing theory and previous models and partly on the experimental results, any sources of error in the experimental measurements will, to some extent, propagate to the model results. When evaluating the overall results, there are at least three plausible explanations for why the simulated results are not more accurate:

1. The suggested relation between statistical time lag, remanent voltage and frequency does not hold.
2. The measurement techniques and post-filtering of the experimental results are not accurate enough; thus, the final results used to estimate the input parameters are flawed.
3. Although numerically inaccurate, the suggested relation is in part correct in describing the phenomenon. However, the assumption of Townsend discharges leads to a very significant difference in numerical values. The impact of different discharge types leads to a large difference, and this simplification limits the model too much.

The selected input parameter values are, as mentioned, chosen based on a *trial and error* method of approach. Different values are selected to see the effects on the PD behaviour when square wave voltage is applied in order to isolate the effects of frequency and voltage rate of change. This allows for a quick investigation into how different values affect the overall behaviour, but it takes a long time to end up with very accurate values. It is also plausible that the actual frequency-dependency is more complex than what can be described with the chosen exponential behaviours. A thorough investigation into the physics of these parameters has not been possible in the limited time available in this master project, hence broad approximations and simplifications were made to investigate the more qualitative change in behaviour than the quantitative.

As covered in section 4.2, subsection 4.3.1 and subsection 4.3.2, extensive work was necessary related to the measurement techniques. Both the available equipment

and post-treatment of the measurements represent significant sources of error that need to be recognised. When measuring the discharge repetition rate by using *peak detection mode* on the oscilloscope, it is possible that some discharges were not registered due to a very short time between discharges. This may, in particular, be the case for streamer-type discharges which are much faster than Townsend-type discharges. Being able to register and separate these in a more efficient way could have led to an even higher discharge rate. When considering the selected method for measuring discharge magnitude, there was, as mentioned, a very limited data sample due to the large resolution. When post-filtering the measurements, some data was also shown to be lost. Further, the test procedure described in section 4.4 represents a source of error. The way in which the test objects are conditioned before a measurement is performed may affect the conditions inside the void to such an extent that the PD behaviour changes. It is known that PDIV may change over time due to a change in void pressure from the ionisation of the gas [24], and that a continuous voltage application may change the PD repetition rate and discharge magnitude [23]. A short conditioning time was selected to decrease the effects of the accumulated charges and a change in gas pressure, and thereby see more clearly the instantaneous effects of the voltage frequency and voltage rate of change. Different approaches to the conditioning may likely have led to other results.

It is almost certainly the case that the assumption of Townsend discharges is partly the reason behind the difference. Firstly, it is of notable interest that the largest difference between the simulation and experimental measurements was found in the repetition rate and not the discharge magnitude. As shown in the PRPD plots in subsection 4.3.1 there is a relatively large spread in discharge magnitude values; PDs of different magnitudes will be present in such voids. For example, one discharge of 1 nC will have the same average discharge magnitude as two discharges of 1.5 nC and 0.5 nC, respectively. However, the number of discharges in these two cases is different. This shows that it is possible to correctly predict the average discharge magnitude without also predicting the repetition rate. Going back to the results presented in this thesis, a far greater number of discharges were measured than simulated, which can be explained by a combination of small-magnitude Townsend discharges and large-magnitude streamer-discharges. Although not extensively investigated in this thesis, it can be seen in Appendix B that discharges of various magnitude and time-span were detected.

Chapter 6

Conclusion

The main objective of the thesis was to explain the voltage frequency- and voltage rate of change-dependency of experimental PD results in cylindrical generator insulation voids.

The results can be summarised in the following points:

- An increase in voltage frequency causes a reduction in PD repetition rate and magnitude. The most significant reduction is seen in the frequency range of 100 - 1500 Hz.
- An increase in voltage rate of change causes a smaller spread in the phase position of PDs.
- An increase in voltage rate of change causes an initial increase in PD repetition rate and magnitude up to 130 V/μs, followed by a reduction when the voltage rate of change is increased further.
- The model, with the selected input parameter values, is able to describe the qualitative behaviour of PD as frequency and voltage rate of change is increased.
- A significant numerical difference in PD repetition rate is observed between the measured and simulated results.

In conclusion, the experimental PD results show a clear dependency on voltage frequency and rate of change. The simplified capacitive abc model is not sufficient to explain the change in PD behaviour, as an implementation of frequency-dependent statistical time lag and remanent voltage is shown to be necessary to obtain similar results in the simulation. At increasing voltage frequencies, it is necessary to reduce the statistical time lag and increase the remanent voltage to obtain the same frequency-dependence in PD repetition rate and magnitude. Further, in order to explain the PDs' dependence on voltage rate of change, it is necessary to decrease the statistical time lag faster and to a lower value, and the remanent voltage has to be reduced to a lower value to allow for larger discharges. The change in statistical time lag can be explained through a change in available electrons caused by a shorter time between discharges, as well as a change in discharge type and void surface characteristics, which affects both the time lag and PD voltage drop.

Significant sources of error in both the laboratory measurements and model input parameter values should be considered when evaluating the results' numerical values. Without a more detailed understanding of the model input parameters, the model will be fundamentally limited in its quantitative predictions. In particular, its assumption of only Townsend-type discharges seems to be at fault.

Chapter 7

Further work

The following suggestions for further work should be considered:

- Collect a larger data-sample by performing measurements on more void geometries. Cylindrical voids with various void gap distances and diameters should be considered, and a large emphasis should be made on the quality in production to avoid uneven surfaces.
- Investigate alternative techniques or other instruments for measuring the PD parameters.
- Investigate in more detail the effects of preconditioning. Understanding how preconditioning affects the results may to both more accurate measurements as well as a more efficient measuring process.
- Implement a field-distribution and field-strength dependency in the PD prediction model to better model the changing behaviour of statistical time lag and charge decay, as well as including different discharge types covering different areas of the void surface.

References

[1] M. N. Johannessen, "Effects of void dimensions and voltage amplitude on partial discharges in generator groundwall insulation," unpublished, 2021.

[2] V. Yaramasu, B. Wu, P. C. Sen, S. Kouro, and M. Narimani, "High-power wind energy conversion systems: State-of-the-art and emerging technologies," *Proceedings of the IEEE*, vol. 103, no. 5, pp. 740–788, 2015. DOI: 10.1109/JPROC.2014.2378692.

[3] S. Ul Haq, S. H. Jayaram, and E. A. Cherney, "Insulation problems in medium-voltage stator coils under fast repetitive voltage pulses," *IEEE Transactions on Industry Applications*, vol. 44, no. 4, pp. 1004–1012, July-aug. 2008. DOI: 10.1109/TIA.2008.926305.

[4] A. Cavallini, D. Fabiani, and G. C. Montanari, "Power electronics and electrical insulation systems [U+07DD] part 1: Phenomenology overview," *IEEE Electrical Insulation Magazine*, vol. 26, no. 3, pp. 7–15, 2010. DOI: 10.1109/MEI.2010.5482783.

[5] ——, "Power electronics and electrical insulation systems - part 2: Life modeling for insulation design," *IEEE Electrical Insulation Magazine*, vol. 26, no. 4, pp. 33–39, 2010. DOI: 10.1109/MEI.2010.5511187.

[6] E. G. Tveten and L. Lundgaard. "Fasttrans: Reducing the impact of repetitive voltage pulses on hv components." (2020), [Online]. Available: https://blog.sintef.com/sintefenergy/electric-power-components/fasttrans-reducing-the-impact-of-repetitive-voltage-pulses-on-hv-components/. accessed: 06.17.2022.

[7] L. Lundgaard. "Fasttrans - insulation stressed with fast rise time repetitive voltages from high voltage power electronics." (2019). accessed: 06.17.2022.

[8] P. Morshuis, "Degradation of solid dielectrics due to internal partial discharge: Some thoughts on progress made and where to go now," *IEEE Transactions*

on Dielectrics and Electrical Insulation, vol. 12, no. 5, pp. 905–913, 2005. DOI: 10.1109/TDEI.2005.1522185.

[9] D. Manns, S. Galioto, K. Weeber, and J. Yagielski, "High frequency life testing of stator coil insulation," in *Conference Record of the 2008 IEEE International Symposium on Electrical Insulation*, 2008, pp. 269–272. DOI: 10.1109/ELINSL.2008.4570326.

[10] W. Chen, G. Gao, and C. A. Mouton, "Stator insulation system evaluation and improvement for medium voltage adjustable speed drive applications," in *2008 55th IEEE Petroleum and Chemical Industry Technical Conference*, 2008, pp. 1–7. DOI: 10.1109/PCICON.2008.4663986.

[11] F. Sahlén, G. Paulsson, and E. Mårtensson, "Life-time investigation of mica-based insulation for high voltage machines subjected to converter-like voltages," in *2016 IEEE Electrical Insulation Conference (EIC)*, 2016, pp. 460–463. DOI: 10.1109/EIC.2016.7548637.

[12] M. S. Moonesan, S. Jayaram, E. Cherney, R. Omranipour, and S. Ul Haq, "Effect of voltage rise time on time-to-failure of form-wound stator coil enamelled turn insulation," in *2014 IEEE Electrical Insulation Conference (EIC)*, 2014, pp. 167–171. DOI: 10.1109/EIC.2014.6869368.

[13] M. S. Moonesan, S. H. Jayaram, and E. A. Cherney, "Time to failure of medium-voltage form-wound machine turn insulation stressed by unipolar square waves," *IEEE Transactions on Dielectrics and Electrical Insulation*, vol. 22, no. 6, pp. 3118–3125, 2015. DOI: 10.1109/TDEI.2015.005201.

[14] ——, "Study on form-wound machine turn insulation subjected to unipolar and bipolar square waves," *IEEE Transactions on Dielectrics and Electrical Insulation*, vol. 23, no. 6, pp. 3242–3248, 2016. DOI: 10.1109/TDEI.2016.005792.

[15] L. Niemeyer, "A generalized approach to partial discharge modeling," *IEEE Transactions on Dielectrics and Electrical Insulation*, vol. 2, no. 4, pp. 510–528, 1995. DOI: 10.1109/94.407017.

[16] P. Morshuis and L. Niemeyer, "Measurement and simulation of discharge induced ageing processes in voids," in *Proceedings of Conference on Electrical Insulation and Dielectric Phenomena - CEIDP '96*, vol. 2, 1996, 520–524 vol.2. DOI: 10.1109/CEIDP.1996.564524.

[17] U. Gafvert, H. Edin, and C. Forssen, "Modelling of partial discharge spectra measured with variable applied frequency," in *Proceedings of the 7th Inter-*

national Conference on Properties and Applications of Dielectric Materials, vol. 3, 2003, 839–842 vol.3. DOI: 10.1109/ICPADM.2003.1218552.

[18] M. Borghei and M. Ghassemi, "Finite element modeling of partial discharge activity within a spherical cavity in a solid dielectric material under fast, repetitive voltage pulses," in *2019 IEEE Electrical Insulation Conference (EIC)*, 2019, pp. 34–37. DOI: 10.1109/EIC43217.2019.9046525.

[19] C. Forssen and H. Edin, "Partial discharges in a cavity at variable applied frequency part 1: Measurements," *IEEE Transactions on Dielectrics and Electrical Insulation*, vol. 15, no. 6, pp. 1601–1609, 2008. DOI: 10.1109/TDEI.2008.4712663.

[20] ——, "Partial discharges in a cavity at variable applied frequency part 2: Measurements and modeling," *IEEE Transactions on Dielectrics and Electrical Insulation*, vol. 15, no. 6, pp. 1610–1616, 2008. DOI: 10.1109/TDEI.2008.4712664.

[21] H. Illias, G. Chen, and P. L. Lewin, "Partial discharge behavior within a spherical cavity in a solid dielectric material as a function of frequency and amplitude of the applied voltage," *IEEE Transactions on Dielectrics and Electrical Insulation*, vol. 18, no. 2, pp. 432–443, 2011. DOI: 10.1109/TDEI.2011.5739447.

[22] G. Callender, T. Tanmaneeprasert, and P. L. Lewin, "Simulating partial discharge activity in a cylindrical void using a model of plasma dynamics," *Journal of Physics D: Applied Physics*, vol. 52, no. 5, p. 055 206, Nov. 2018. DOI: 10.1088/1361-6463/aaedf0. [Online]. Available: https://doi.org/10.1088/1361-6463/aaedf0.

[23] T. G. Aakre, "Partial discharges in voids at variable voltage frequency and temperature diagnostic testing of stator mainwall insulation," Ph.D. dissertation, Dept. Elect. Power Eng., NTNU, Trondheim, Norway, 2020. [Online]. Available: https://hdl.handle.net/11250/2651660.

[24] CIGRÉ WG D1.33, *Guide for partial discharge measurements in compliance to IEC 60270*, No. 366, 2008.

[25] C. Pan, G. Chen, J. Tang, and K. Wu, "Numerical modeling of partial discharges in a solid dielectric-bounded cavity: A review," *IEEE Transactions on Dielectrics and Electrical Insulation*, vol. 26, no. 3, pp. 981–1000, 2019. DOI: 10.1109/TDEI.2019.007945.

[26] E. Kuffel, W. S. Zaengl, and J. Kuffel, *High voltage engineering : fundamentals*, eng, 2nd ed. Boston: Butterworth-Heinemann, 2000, ISBN: 1-281-07270-2.

[27] P. K. Olsen, "Internal partial discharges at high dc voltage and the effect of superimposed ac voltage," eng, Ph.D. dissertation, 2020, ISBN: 978-82-326-5001-9. [Online]. Available: https://hdl.handle.net/11250/2682477.

[28] J. C. Devins, "The 1984 J. B. Whitehead memorial lecture the physics of partial discharges in solid dielectrics," *IEEE Transactions on Electrical Insulation*, vol. EI-19, no. 5, pp. 475–495, 1984. DOI: 10.1109/TEI.1984.298770.

Appendix A

Impact of model input parameter values

The impact of voltage frequency and rate of change on the PD behaviour is investigated through the experimentation of different values for τ_s, τ_{rel} and U_{rem}. Each parameter affects the PD repetition rate and magnitude in its own way; a selection of values is shown here to demonstrate the core change in behaviour with various values for these parameters. The selected voltage used here was with a square wave voltage with voltage amplitude equal to 10% above the PDIV in TO3, and the void geometry was equal to that of TO3. The rise time was set to 130 μs. The plots that are shown here are with the average values of 18 simulations, along with the maximum and minimum values (errorbars) at each frequency to illustrate the potential spread caused by statistical time lag.

A.1 Statistical time lag

The impact of the statistical time lag value on the PD behaviour using the implemented model can be seen in Figure A.1.1 and Figure A.1.2. A constant parameter value for charge decay and remanent voltage is used to highlight the impact of statistical time lag only; $\tau_{rel} = 0.01$ and $U_{rem} = U_{paschen} \cdot 0.8$. The largest impact is seen on the PD repetition rate, where a constant τ_s gives a larger drop in repetition rate when the frequency is increased. Using a smaller, but still constant value gives a higher repetition rate at the high frequencies due to the time lag being smaller relative to the voltage period. At very low values like 0.1 ms, the time lag on voltage frequencies below 1 kHz becomes essentially negligible compared with the voltage period, so the repetition rate remains (relatively) flat

until it starts to drop. Lastly, an exponentially decreasing statistical time lag proposed in Equation 3.2 with $\tau_{s,min}$=0.25 ms and λ=0.003 is used as an example of how a decreasing time lag would affect the PD results. The repetition rate is decreasing, but more linearly compared with a constant τ_s value. A larger drop (higher λ and/or lower $\tau_{s,min}$) leads to smaller drop in repetition rate with increasing frequency.

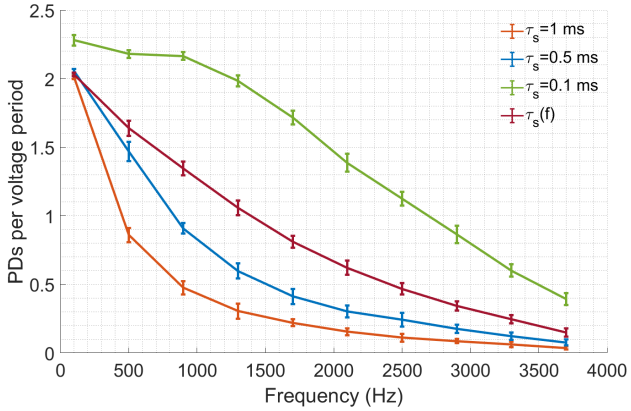

Figure A.1.1: Impact of various statistical time lag values on PD repetition rate

The impact of various values for τ_s is very small on the discharge magnitude, although a larger value seems to decrease the magnitude somewhat on larger frequencies above 1 kHz. This can be explained by the fact that a square wave voltage remains at its maximum amplitude for a large part of the period, so any time lag above a certain level will lead to discharges from the same voltage amplitude, giving small differences in discharge magnitude.

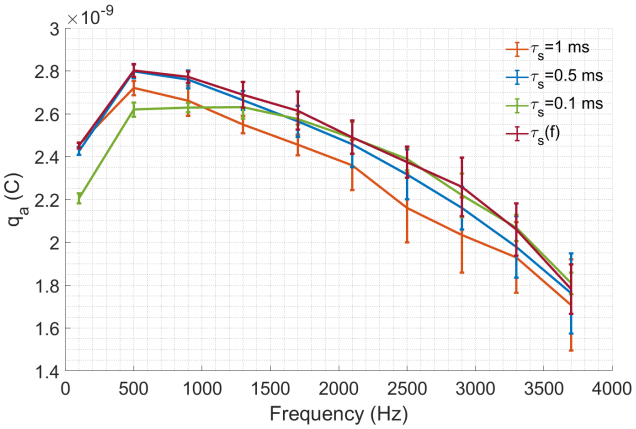

Figure A.1.2: Impact of various statistical time lag values on PD magnitude

A.2 Charge decay

The impact of charge decay is shown in Figure A.2.1 and Figure A.2.2, where three values of τ_{rel} are used. A smaller relaxation time constant means that the residual voltage will decay faster, thereby restoring the voltage quicker. The impact is negligible on the PD repetition rate, which is due to the impact of statistical time lag, which is dominating on the repetition rate. The impact of a short relaxation time constant in noticeable on the PD magnitude, where it start at a lower value at 100 Hz with an initial increase followed by a decline. Because a square wave voltage will maintain its maximum amplitude for a relatively long time, the charge decay has an effect on the residual voltage in this section of the period between the last PD even and the following zero-crossing. At a low frequency and with a fast decay, this has a noticeable effect. As frequency is increased, the time spent at maximum amplitude becomes short enough that the charge decay does not have time to affect the residual voltage, so the impact becomes smaller and smaller.

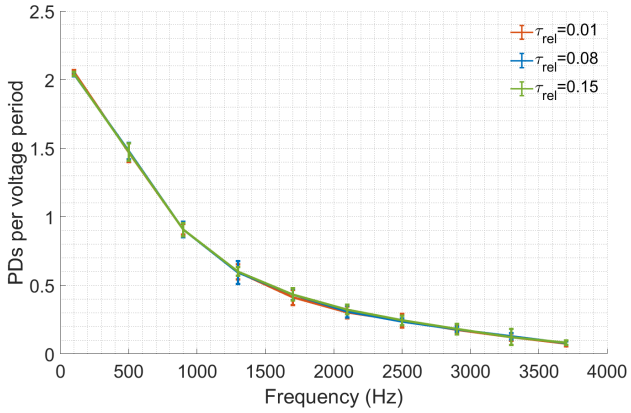

Figure A.2.1: Impact of various relaxation time constants on PD repetition rate

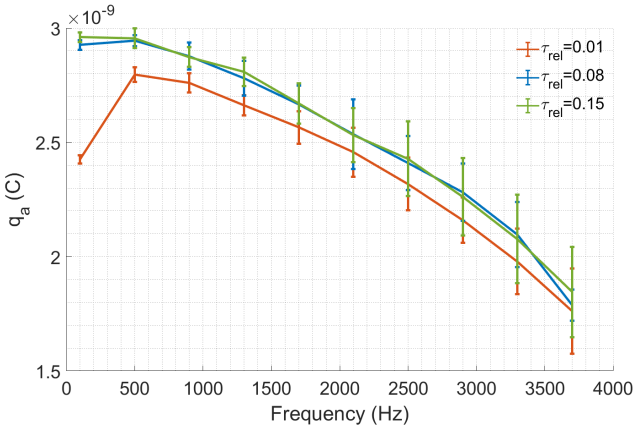

Figure A.2.2: Impact of various relaxation time constants on PD magnitude

A.3 Remanent voltage

The impact of various values for α, which is used to find U_{rem}, is seen in Figure A.3.1 and Figure A.3.2. Apart from a high α-value of 0.95, the impact on the PD repetition rate is negligible. The impact on the discharge magnitude is however significant and follows the expected pattern.

A large remanent voltage means that the voltage drop is significantly lower, leading to a smaller discharge magnitude as well as higher repetition rate due to the residual voltage being closer to the critical level after a discharge; it takes less time to reach the critical level again. By selecting a constant remanent voltage level, the discharge magnitude decreases with increasing frequency due to the effect of time lag. When a frequency-dependent remanent voltage is selected, there is no initial increase in discharge magnitude, only a continuous decrease. This is because the initial α value is relatively small but decreases quickly, leading to a significant drop in voltage drop magnitude. This counteracts the initial increase caused by the time lag.

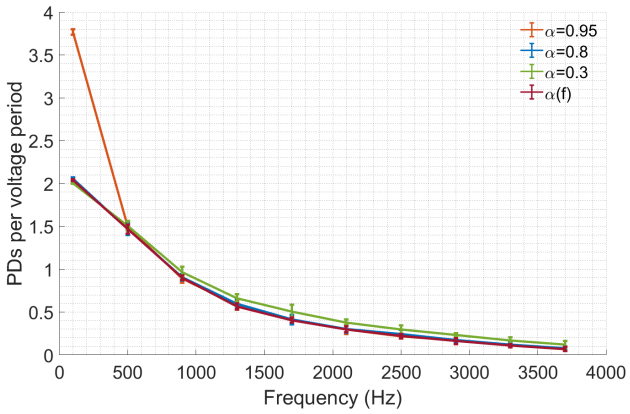

Figure A.3.1: Impact of various values of remanent voltage on PD repetition rate

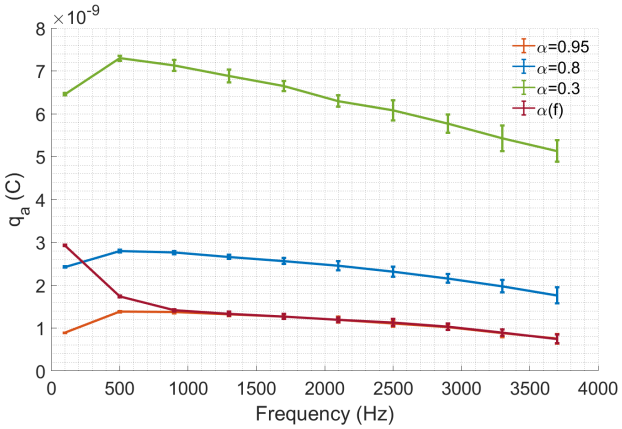

Figure A.3.2: Impact of various values of remanent voltage on PD magnitude

Appendix B

Additional results

B.1 Measurements on test object 1

As seen in Figure B.1.1, Figure B.1.2 and Figure B.1.3, measurements were performed on TO7 at sine wave voltage using MPD 600. The measurements shows that the PD magnitudes are very small; less than 300 pC. In addition, the discharge repetition rate is very low; less than 1 PD per voltage cycle with 100 Hz and 500 Hz, and 1.16 PDs per voltage cycle at 900 Hz.

The combination of very small discharge magnitudes and a low repetition rates makes it unfeasible to apply the same post-processing procedure on these measurements as with TO8 and TO9. The low repetition rate makes the number of discharges available for integration (to find discharge magnitude) very low, and the low discharge magnitude makes it far more challenging to separate from noise.

Efforts were made to measure and process the data with the same voltages as investigated in the thesis, but the results made it clear that it was not possible to draw any valid conclusions or comparisons from. Figure B.1.4 shows how, even if PDs are possible to detect visually, most of the pulse falls withing the limits of the noise and is therefore difficult to isolate. A more sophisticated method of post-filtering would be required. Lastly, in Figure B.1.5 shows how the cumulative integration ends up if an effort is made to filter the noise. Substantial parts of the noise are still present, leading to multiple changes in the integration between the actual discharges. It should be noted that the results became even more difficult to process at higher frequencies, as the discharge magnitudes became even lower.

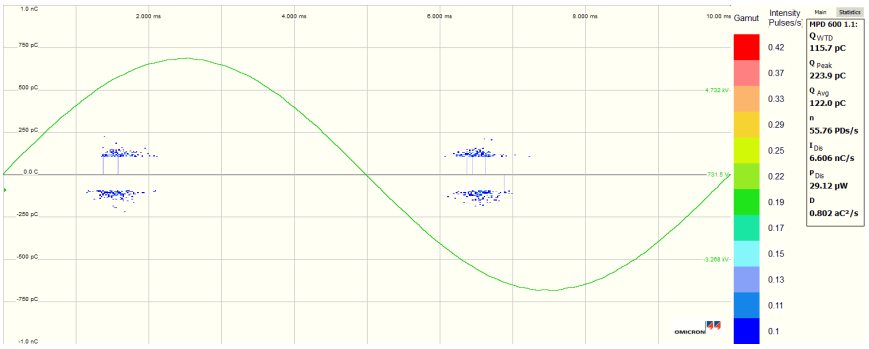

Figure B.1.1: Measurement with MPD 600 on TO1 at 100 Hz sine wave voltage

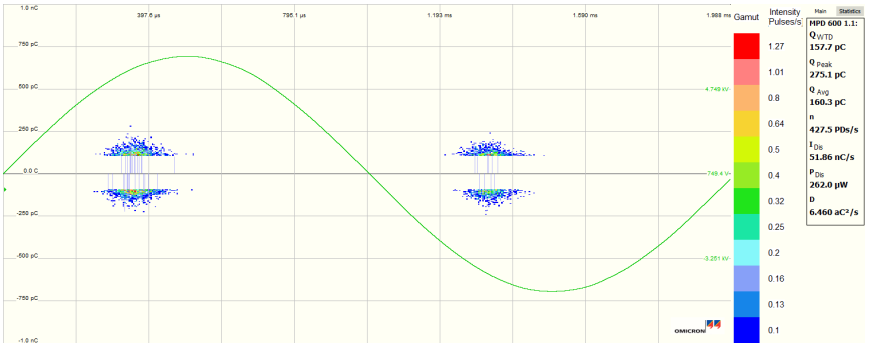

Figure B.1.2: Measurement with MPD 600 on TO1 at 500 Hz sine wave voltage

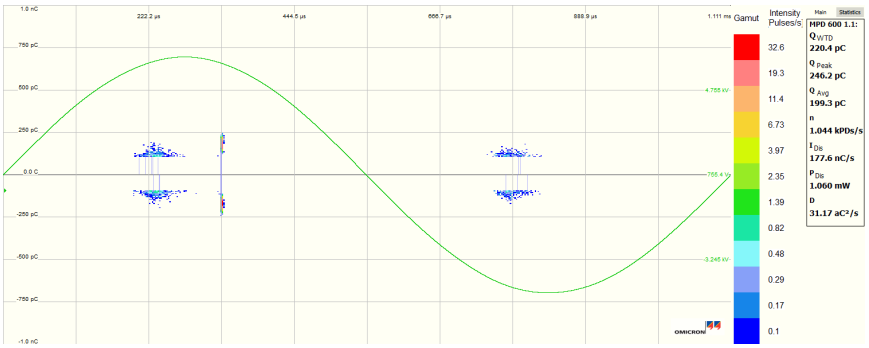

Figure B.1.3: Measurement with MPD 600 on TO1 at 900 Hz sine wave voltage

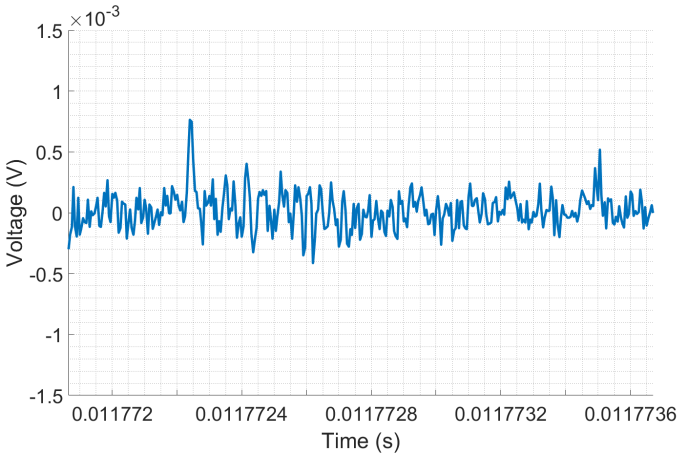

Figure B.1.4: PD voltage pulse in TO7 at 100 Hz sine wave voltage

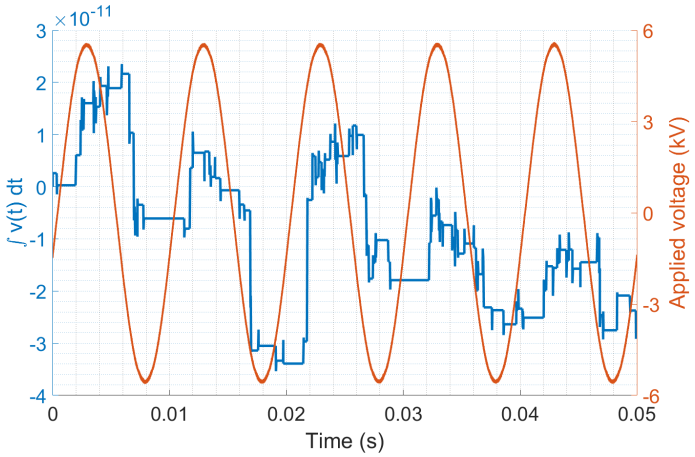

Figure B.1.5: Cumulative integration of PD pulses in TO7 at 100 Hz sine wave voltage

B.2 Oscilloscope measurements

Here, a selection of screenshots from the measurements on the oscilloscope is shown to illustrate how the original measurements were taken.

B.2.1 PD detection

The presence of PDs are clearly observed with both sine wave and square wave voltage, as seen from Figure B.2.1 and Figure B.2.2. In Figure B.2.3, the capacitive current is shown to cause a ripple in the sections where the voltage is rising and falling, showing the need to include a digital highpass filter to exclude this ripple from the discharges, allowing for the subsequent implementation of a noise threshold.

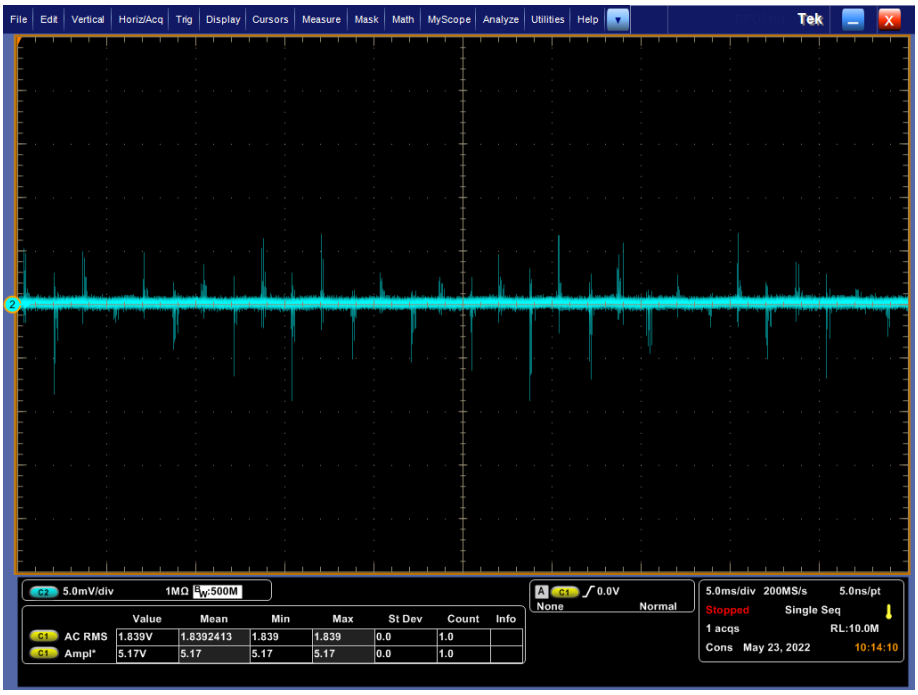

Figure B.2.1: Oscilloscope screenshot with 300 Hz sine wave voltage

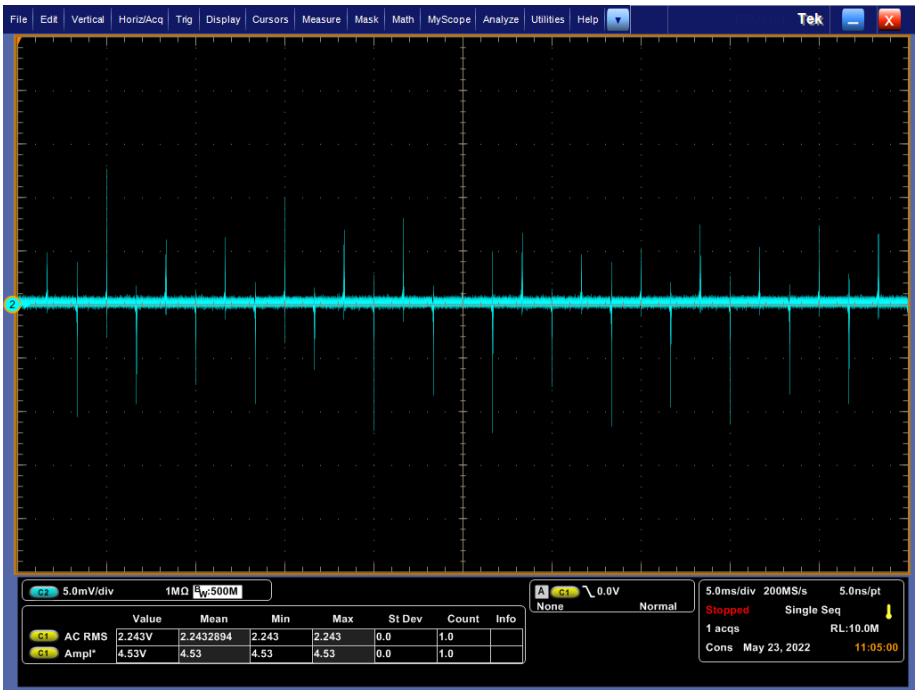

Figure B.2.2: Oscilloscope screenshot with 300 Hz square wave voltage, with a 300 pF parallel capacitor

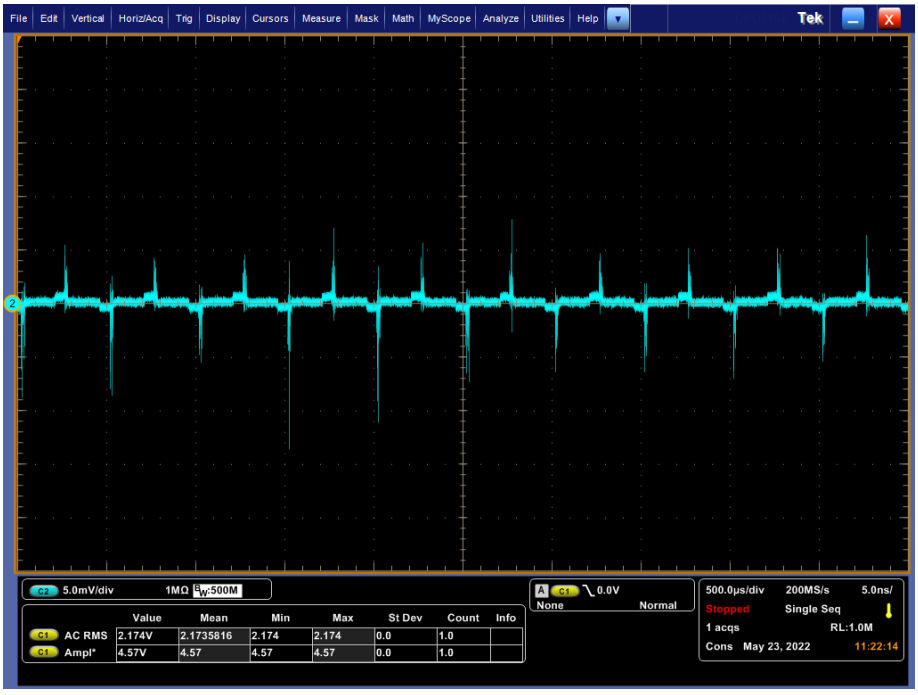

Figure B.2.3: Oscilloscope screenshot with 2000 Hz square wave voltage, with a 300 pF parallel capacitor

B.2.2 Voltage rise time and rate of change

The voltage rate of change is found by measuring the rise time and voltage difference with each parallel capacitor. The measurements are done on the oscilloscope as shown in Figure B.2.4, Figure B.2.5 and Figure B.2.6. The rise times are, by default, measured from the 10% mark to the 90% mark of the rising flank. The voltage difference in this same time period is measured and shown as ΔV. It should be noted that the voltage is reduced by a fraction of 2000 to the oscilloscope, so the voltage rate of change (in kV/μs) is then calculated as

$$dV/dT = \frac{2000 \cdot \Delta V}{Rise\ time}$$

in each case.

Figure B.2.4: Oscilloscope screenshot with 50 Hz square wave voltage, with a 1 nF parallel capacitor, showing the measurement of rise time

Figure B.2.5: Oscilloscope screenshot with 50 Hz square wave voltage, with a 300 pF parallel capacitor, showing the measurement of rise time

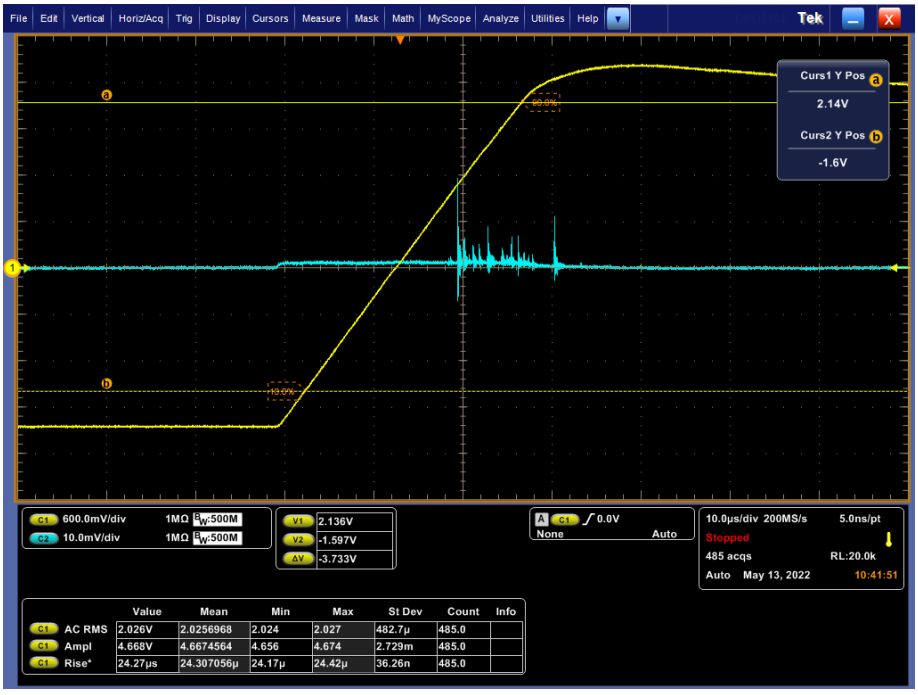

Figure B.2.6: Oscilloscope screenshot with 50 Hz square wave voltage, with no parallel capacitor

B.3 Measured PD pulses

A selection of measured PD pulses is shown here to demonstrate that pulses of various magnitude and duration were present in the test objects.

A selection of measured PD pulses are shown in Figure B.3.1, Figure B.3.2 and Figure B.3.3, where a sine wave voltage at 1100 Hz is applied to TO3. Comparing these with measurements at square wave voltage in Figure B.3.4, Figure B.3.5 and Figure B.3.6 with the same frequency and a large voltage rate of change (300 V/μs), a clear change in time between discharges as well as discharge behaviour is observed. When a faster voltage is applied, the time between discharges is reduced dramatically, and the pulse magnitudes are generally much higher. With the square wave voltage, a much larger difference in PD types are observed; both long- and short-lasting pulses with various magnitudes are present.

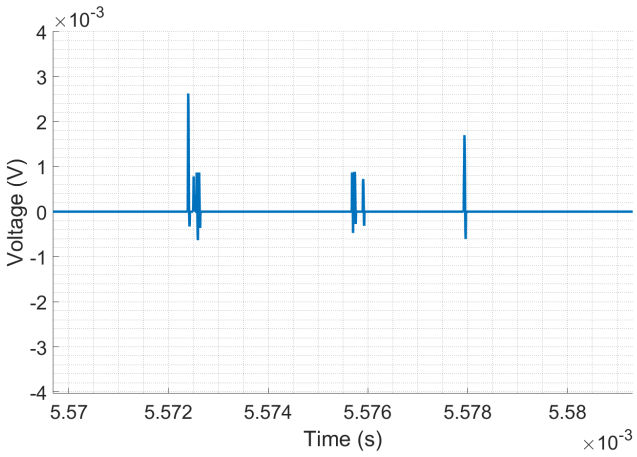

Figure B.3.1: PD pulses in TO3 with sine wave voltage at 1100 Hz

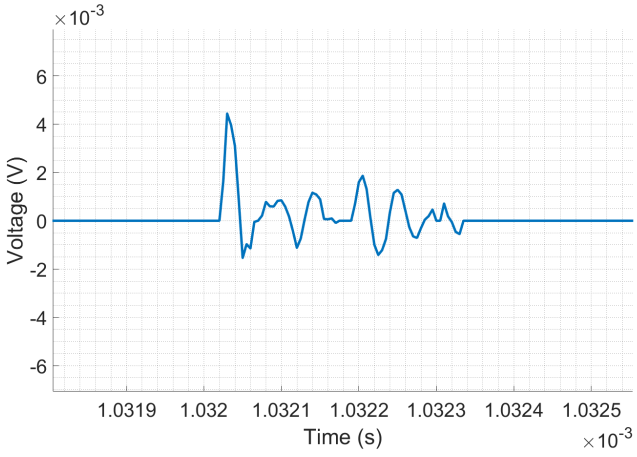

Figure B.3.2: PD pulses in TO3 with sine wave voltage at 1100 Hz

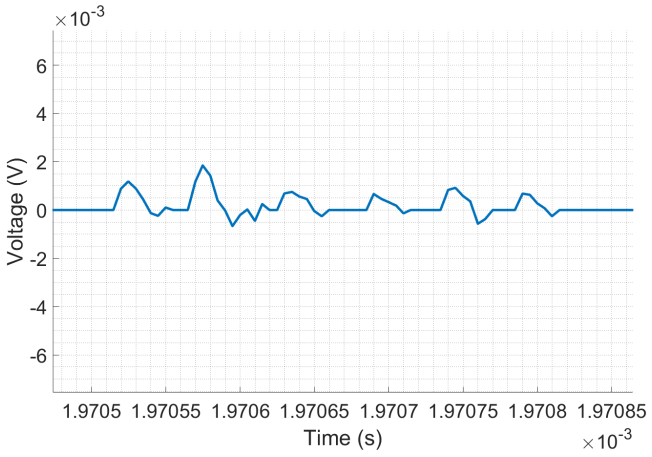

Figure B.3.3: PD pulses in TO3 with sine wave voltage at 1100 Hz

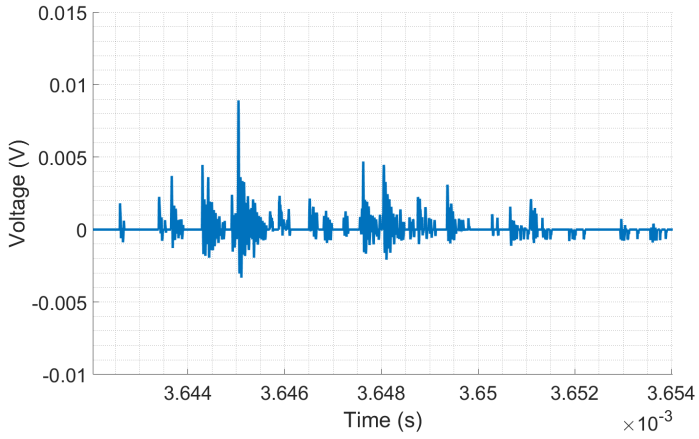

Figure B.3.4: PD pulses in TO3 with square wave voltage at 1100 Hz with no parallel capacitor

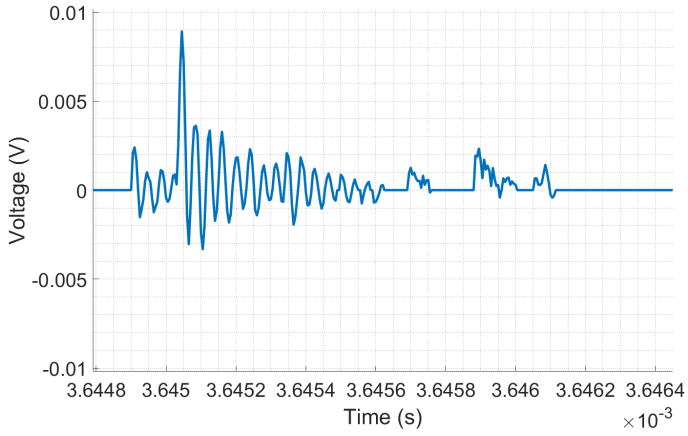

Figure B.3.5: PD pulses in TO3 with square wave voltage at 1100 Hz with no parallel capacitor

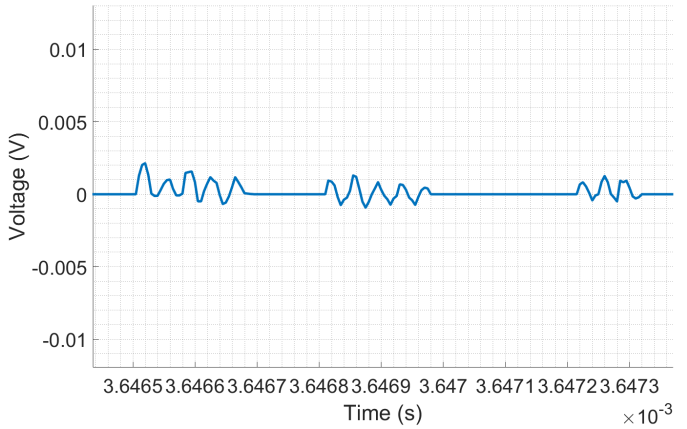

Figure B.3.6: PD pulses in TO3 with square wave voltage at 1100 Hz with no parallel capacitor

Appendix C

Model code

C.0.1 PD prediction model with square wave voltage

```
d_a=2;      %Test object thickness
d_c=0.52;   %Void gap distance
r_c=10e-3;  %Void radius
d_b=d_a-d_c;%Series dielectric thickness
eps_b=3.94; %Dielectric permittivity
eps_c=1;    %Air permittivity
eps_0=8.854187e-12; %Vacuum permittivity
C_b=(eps_0*eps_b*(pi*r_c^2)/(d_b*1e-3))*1e3; %1e-3 for mm, ...
    multiplication with 1000 because voltage is in kV.

rho_0=0.9961; %Temperature factor
U_crit=@(d) (2.436.*(rho_0.*d)+2.125.*sqrt(rho_0.*d)); %Function...
     for paschen voltage
U_pasch=U_crit(d_c); %Paschen voltage in 2mm insulation for the ...
    given void gap
U_pdiv = U_pasch*(1+((d_b)/d_c)*(eps_c/eps_b)); %Applied voltage...
     at critical field strength, i.e. PDIV

U_a=U_pdiv*1.1; %Applied voltage, kV peak
U_v0=(U_a)/(1+((d_b)/d_c)*(eps_c/eps_b)); %Void voltage

A_pp = U_v0*2;  %Amplitude, peak-peak
D=0.5;          %Duty-cycle
tau_r = 130e-6; %Rise-time. 30, 70 or 280 us.
t_shift = tau_r/2; %Time shift so that F(0)=0
N=200;    %Partial harmonics

tau_rel=0.01; %Charge decay constant (high value = low decay ...
    rate)
```

```
25
26 %Frequency vector
27 f_start=100;
28 f_step=400;
29 f_stop=3700;
30
31 P=500;  %Numer of voltage cycles to simulate
32 parfor u=1:18 %Number of parallel simulations
33     Bn=zeros(1,1); %Matrix for storing the number of discharges ...
           at each frequency for all parallel loops
34     Ba=zeros(1,1); %Matrix for storing the PD magntiude at each ...
           frequency for all parallel loops
35     f_k=1;  %Counter for iterations
36     tL_max=zeros(1,1);  %Matrix for maximum values of time lag ...
           (1/2 voltage period)
37     tL=zeros(1,1); %Matrix for storing time lag values at each ...
           frequency
38
39     %Creating a matrix of time lag values at all frequencies:
40     for f=f_start:f_step:f_stop
41         T=1/f;
42         tL_max(1,f_k)=T/2;
43         t_s=1e-3*(0.015+0.385*exp(-0.003*f));
44         for i=1:50000
45             tL(i,f_k)=-t_s*log(1-rand());
46             if tL(i,f_k)>tL_max(1,f_k)
47                 tL(i,f_k)=tL_max(1,f_k);
48             end
49         end
50         f_k=f_k+1;
51     end
52     B=zeros(1,1); %Matrix for storing void voltage values in ...
           each time step. Necessary to check for polarity change
53     f_k=1; %Counter for iterations
54     for f=f_start:f_step:f_stop
55         alpha=(0.95/(1+exp(-0.005*(f+250))));
56         U_rem=U_pasch*alpha; %Remanent voltage
57         dV=0;
58         Fs=5e6;
59         T=1/f;
60         tau = T*D;
61
62         %Adjusting number of partial harmonics to frequency. At ...
               higher
63         %frequency, a lower N is required to obtain an ...
               acceptable shape.
64         %Lower N is preferrable to reduce computation time.
65         if f<400
66             n=1:300;
```

```
67          else
68              n=1:100;
69          end
70          %Creating the trapezoid voltage function:
71          F_sq = @(t) -A_pp/2 + A_pp*(tau/T) + 2*A_pp*(tau/T) .* ...
                sum( (sin(n(:)*pi*f*tau)./(n(:)*pi*f*tau)) .* (sin(n...
                (:)*pi*f*tau_r)./(n(:)*pi*f*tau_r)) .* cos(2*pi*n(:)...
                *f*(t-t_shift)-pi*n(:)*f*(tau-tau_r)) ) ;
72
73          Ures=0; %Residual voltage
74          Q=zeros(1,1); %Vector of dicharge magnitudes
75          k=1; %Counter for discharge events
76          kp=1 %Positive discharge events
77          kL=1; %Counter for time-lags
78          it=1; %Counter for time-step
79          t_q=zeros(1,1); %Vector of times between discharges
80          dv=0; %Voltage drop from time-step value to Urem
81          for t=0:1/Fs:P*T
82              Uvoid_0=F_sq(t); %Void voltage assuming no ...
                    discharges
83              Uvoid= Uvoid_0 + Ures; %Void voltage including ...
                    dischages
84              B(it,1)=Uvoid;
85              if (F_sq(t-tL(kL,f_k))+Ures ≥ U_pasch) && (Uvoid≥...
                    U_pasch)
86                  dv=Ures-Uvoid+U_rem;
87                  Ures=Ures-Uvoid+U_rem;
88                  dV=-Uvoid+U_rem;
89                  Q(k)=dV*C_b;
90                  t_q(k,1)=t;
91                  k=k+1;
92                  kL=kL+1;
93              elseif (F_sq(t-tL(kL,f_k))+Ures ≤ -U_pasch) && (...
                    Uvoid≤-U_pasch)
94                  dv=Ures-Uvoid-U_rem;
95                  Ures=Ures-Uvoid-U_rem;
96                  dV=-Uvoid-U_rem;
97                  Q(k)=dV*C_b;
98                  t_q(k,1)=t;
99                  k=k+1;
100                 kp=kp+1;
101                 kL=kL+1;
102             end
103             %New time-lag if voltage polarity changes:
104             if t>(T/2) && ( sign(B(it,1)) ≠ sign(B(it-1,1)) )
105                 kL=kL+1;
106             end
107             k2=length(t_q);
108             dt=t-t_q(k2,1); %Time since previous discharge
```

```
109             Ures=dv*exp(-dt/tau_rel); %Charge decay on residual ...
                    voltage
110             it=it+1;
111         end
112
113         Bn(f_k)=length(Q);
114         Ba(f_k)=mean(abs(Q));
115         f_k=f_k+1;
116     end
117     Qn(:,u)=Bn;
118     Qa(:,u)=Ba;
119 end
```

C.0.2 PD prediction model with sine wave voltage

```
%% Setting voltage parameters and time-lag
d_a=2;      %Test object thickness
d_c=0.52;   %Void gap distance
r_c=10e-3;  %Void radius
d_b=d_a-d_c;%Series dielectric thickness
eps_b=3.94; %Dielectric permittivity
eps_c=1;    %Air permittivity
eps_0=8.854187e-12; %Vacuum permittivity
C_b=(eps_0*eps_b*(pi*r_c^2)/(d_b*1e-3))*1e3; %1e-3 for mm, ...
    multiplication with 1000 because voltage is in kV.

rho_0=0.9961; %Temperature factor
U_crit=@(d) (2.436.*(rho_0.*d)+2.125.*sqrt(rho_0.*d)); %Function...
     for paschen voltage
U_pasch=U_crit(d_c); %Paschen voltage in 2mm insulation for the ...
    given void gap
U_pdiv = U_pasch*(1+((d_b)/d_c)*(eps_c/eps_b)); %Applied voltage...
     at critical field strength, i.e. PDIV

U_a=U_pdiv*1.1;    %Applied voltage,kV peak
U_v0=(U_a)/(1+((d_b)/d_c)*(eps_c/eps_b)); %Void voltage at ...
    applied voltage

tau_rel=0.01; %Charge decay constant (high value = low decay ...
    rate)

%Frequency vector
f_start=100;
f_step=200;
f_stop=1500;


P=500;  %Numer of voltage cycles to simulate
parfor u=1:18 %Number of parallel simulations
    Bn=zeros(1,1); %Matrix for storing the number of discharges ...
        at each frequency for all parallel loops
    Ba=zeros(1,1); %Matrix for storing the PD magntiude at each ...
        frequency for all parallel loops
    f_k=1;  %Counter for iterations
    tL_max=zeros(1,1);  %Matrix for maximum values of time lag ...
        (1/2 voltage period)
    tL=zeros(1,1); %Matrix for storing time lag values at each ...
        frequency

    %Creating a matrix of time lag values at all frequencies:
    for f=f_start:f_step:f_stop
```

```
37          T=1/f;
38          tL_max(1,f_k)=T/2;
39          t_s=1e-3*(0.25+0.75*exp(-0.0008*f));
40          for i=1:50000
41              tL(i,f_k)=-t_s*log(1-rand());
42              if tL(i,f_k)>tL_max(1,f_k)
43                  tL(i,f_k)=tL_max(1,f_k);
44              end
45          end
46          f_k=f_k+1;
47      end
48      B=zeros(1,1); %Matrix for storing void voltage values in ...
            each time step. Necessary to check for polarity change
49      f_k=1; %Counter for iterations
50      for f=f_start:f_step:f_stop
51          alpha=(0.95/(1+exp(-0.0015*(f+2500))));
52          U_rem=U_pasch*alpha; %Remanent voltage
53          dV=0;
54          Fs=5e6;
55          T=1/f;
56          Ures=0; %Residual voltage
57          Q=zeros(1,1); %Vector of dicharge magnitudes
58          k=1; %Counter for discharge events
59          kp=1 %Positive discharge events
60          kL=1; %Counter for time-lags
61          it=1; %Counter for time-step
62          t_q=zeros(1,1); %Vector of times between discharges
63          dv=0; %Voltage drop from time-step value to Urem
64          for t=0:1/Fs:P*T
65              Uvoid_0=U_v0*sin(2*pi*f*t); %Void voltage assuming ...
                    no discharges
66              Uvoid= Uvoid_0 + Ures; %Void voltage including ...
                    dischages
67              B(it,1)=Uvoid;
68              if ((U_v0*sin(2*pi*f*(t-tL(kL,f_k)))+Ures) ≥ U_pasch...
                    ) && (Uvoid≥U_pasch)
69                  dv=Ures-Uvoid+U_rem;
70                  Ures=Ures-Uvoid+U_rem;
71                  dV=-Uvoid+U_rem;
72                  Q(k)=dV*C_b;
73                  t_q(k,1)=t;
74                  k=k+1;
75                  kL=kL+1;
76              elseif ((U_v0*sin(2*pi*f*(t-tL(kL,f_k)))+Ures) ≤ -...
                    U_pasch) && (Uvoid≤-U_pasch)
77                  dv=Ures-Uvoid-U_rem;
78                  Ures=Ures-Uvoid-U_rem;
79                  dV=-Uvoid-U_rem;
80                  Q(k)=dV*C_b;
```

```
81                  t_q(k,1)=t;
82                  k=k+1;
83                  kp=kp+1;
84                  kL=kL+1;
85              end
86              %New time-lag if voltage polarity changes:
87              if t>(T/2) && ( sign(B(it,1)) ≠ sign(B(it-1,1)) )
88                  kL=kL+1;
89              end
90              k2=length(t_q);
91              dt=t-t_q(k2,1); %Time since previous discharge
92              Ures=dv*exp(-dt/tau_rel); %Charge decay on residual ...
                    voltage
93              it=it+1;
94          end
95
96          Bn(f_k)=length(Q);
97          Ba(f_k)=mean(abs(Q));
98          f_k=f_k+1;
99      end
100     Qn(:,u)=Bn;
101     Qa(:,u)=Ba;
102 end
```

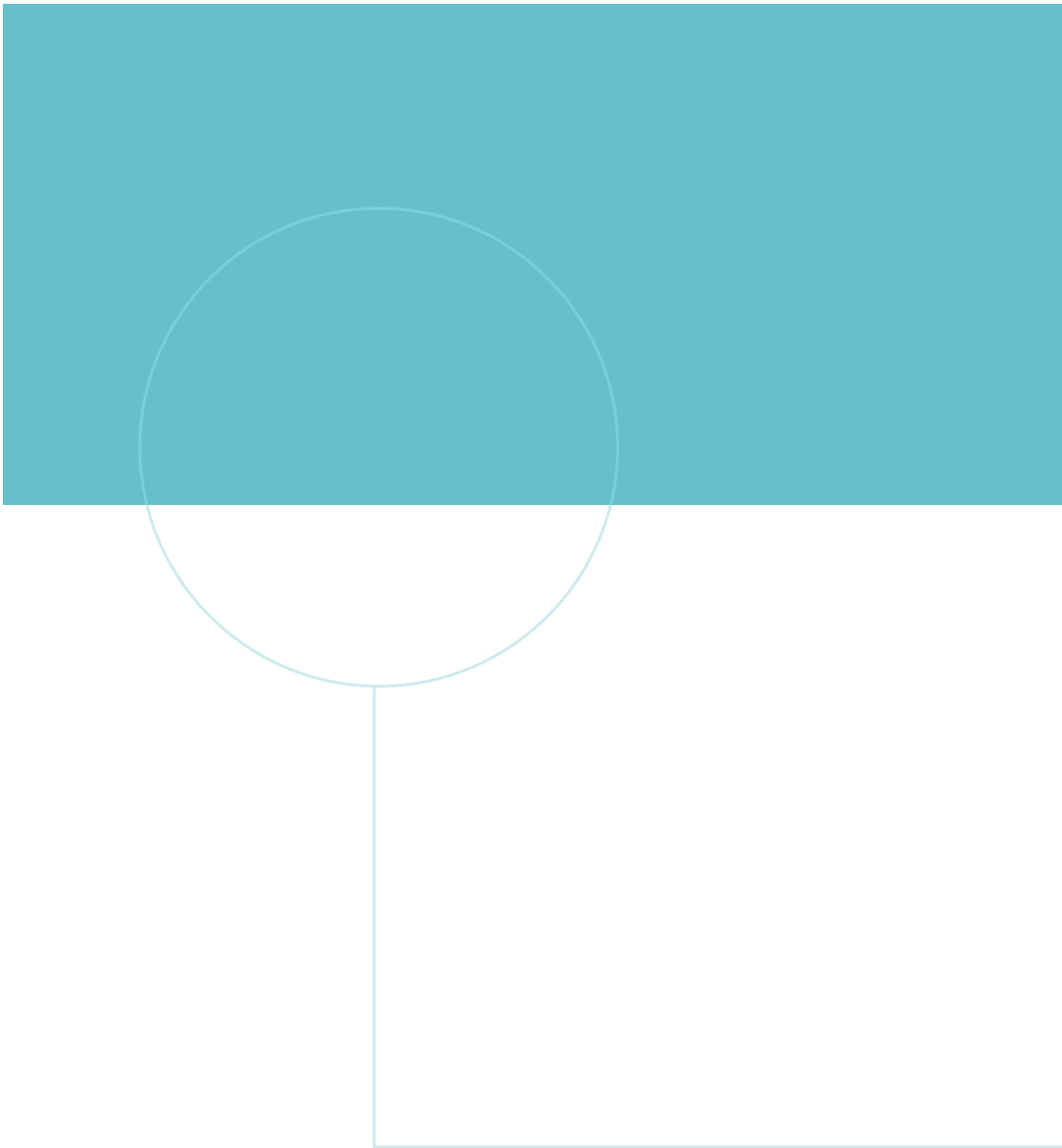

NTNU

Norwegian University of
Science and Technology